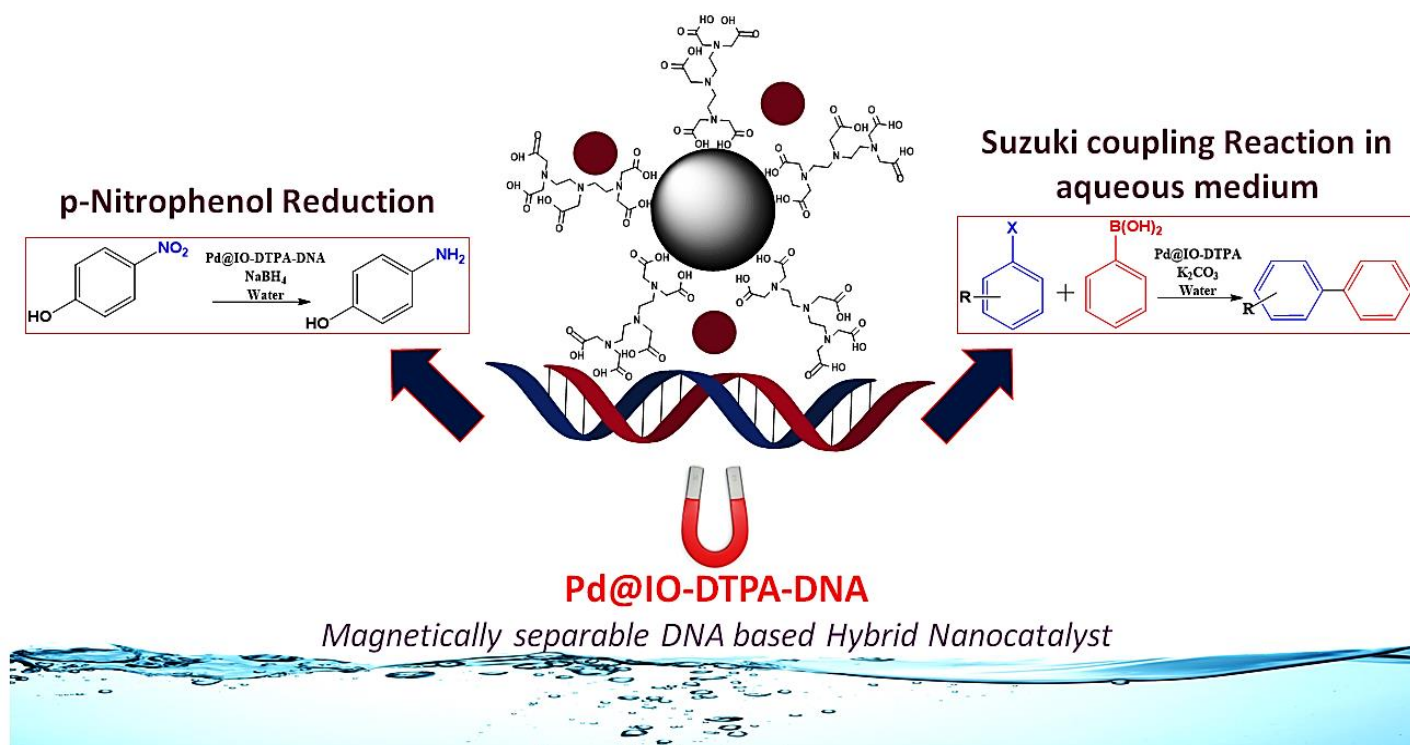




Chapter 6: DNA based magnetically separable hybrid Nanocatalyst: Preparation, Characterization and Applications



6.1. Introduction

The combination of biopolymers like proteins and polynucleotides with the catalytic power of transition metals has emerged as a new generation of hybrid catalysts (Boersma et al., 2007).

Covalent anchoring or supramolecular (non-covalent) anchoring are the two main techniques used to attach a catalytically active metal (transition metal) to prepare DNA-based hybrid catalysis. The ability of DNA to bind with small molecules via hydrophobic, π -stacking, electrostatic, and/or hydrogen bonding interactions can be taken as an advantage to create supramolecular anchoring through intercalation and/or groove binding of metal complex with DNA. Covalent anchoring involves attaching a transition metal to the DNA through a short spacer moiety in the ligand (Boersma et al., 2010).

However, very few researchers have worked on the application of these catalysts in Suzuki C-C coupling reactions. Mart et al. had synthesized Pd/DNA catalyst by using salmon fish sperm DNA and $(\text{Pd}(\text{OAc})_2$ and PdCl_2) as palladium precursor. This homogenous catalyst was used for the Suzuki coupling reaction. Pd/DNA was recovered by simple phase separation and showed recyclability up to 7 cycles (Mart et al., 2018). Kandathil et al., synthesized DNA supported on silane functionalized magnetite, and then used it to graft palladium nanoparticles. This prepared bio-nanocatalyst was further used as magnetically recoverable catalyst for Suzuki–Miyaura cross-coupling reaction. They could have achieved the recyclability up to six cycles (Kandathil et al., 2020). Qu et al., utilized Calf thymus DNA for synthesising stable aqueous suspensions of graphene sheets after which Pd nanoparticles were anchored on it (DNA-G-Pd), which was used for Formic Acid Electro-Oxidation and for the Suzuki Reaction and could be recycled up to seven cycles (Qu et al., 2012). Chakraborty et al., demonstrated a route for the synthesis of Pd and Fe_3O_4 functionalized DNA (Sodium salt of salmon milt deoxyribonucleic acid, (sm-DNA)) in deep eutectic solvent (DES) where DES acts as a media for DNA metallization as well as a solvent for Suzuki coupling reaction and reduction of Nitrobenzene. wherein the catalyst showed recyclability up to six cycles (Chakraborty et al., 2019).

In continuation with our investigation on DTPA and biobased Pd catalysts (chapters 3 and 5) our interest in the present chapter was directed towards the use of DNA instead of chitosan to prepare magnetically recoverable IO-DTPA-DNA catalyst. DNA was sourced from Calf thymus (CT-DNA), Pd@IO-DTPA-DNA was used as a magnetically recoverable

nanocatalyst for Suzuki coupling reaction in aqueous medium as well as for the p-Nitrophenol reduction reaction.

6.2. Materials and methods

6.2.1. Materials

CT-DNA was purchased from Sigma Aldrich.

6.2.2. Procedure for the preparation of DTPA capped Iron oxide nanoparticles (IO-DTPA)

The IO-DTPA was prepared via chemical co-precipitation method as described in Chapter 5 section 5.2.2.

6.2.3. Procedure for the Capping of DNA on IO-DTPA (IO-DTPA-DNA)

IO-DTPA-DNA was synthesized by treating a suspension of 50 mg IO-DTPA in 100 ml water with 2 mL 0.35 mmol CT-DNA solution for 12 h. The resultant IO-DTPA-DNA nanoparticles were separated with a magnet, washed with water and finally dried at 100 °C for 7-8 h.

6.2.4. Procedure for the immobilization of Pd on IO-DTPA-DNA (Pd@IO-DTPA-DNA)

Pd@IO-DTPA-DNA was prepared by sonicating a suspension containing 100 mg IO-DTPA-DNA in 20 ml ethanol for 20 min followed by the addition of 2 mg PdCl₂ to the suspension with gentle stirring for 12h. The resultant Pd@IO-DTPA-DNA nanoparticles were separated with a magnet, washed with ethanol and finally dried at 100 °C for 5 h.

6.2.5. General procedure for the Suzuki coupling reaction using Pd@IO-DTPA-DNA catalyst

A 25 mL round-bottomed flask was charged with aryl halide (1.59 mmol), arylboronic acid (1.59 mmol), K₂CO₃ (1.59 mmol), Pd@IO-DTPA-DNA (1 mg) and H₂O (10 mL). The reaction mixture was placed on an oil bath at 90-100 °C and stirred for 6 to 15 h depending on the aryl halides used. The reaction was monitored by thin layer chromatography (TLC). After completion of the reaction the mixture was cooled to room temperature. Subsequently, the mixture was extracted with ethyl acetate three times (3*5 ml). The catalyst was removed using an external magnet. The ethyl acetate phase was then collected, dried with Na₂SO₄ and the solvent removed under reduced pressure to get the crude product.

TLC analyses were performed to monitor the reaction. The obtained crude product was analysed by GC-MS. Chromatography purifications were carried out with using column chromatography packed by silica gel (230–400 mesh) and Enantiomeric excesses (ee) of axially chiral compounds were determined by HPLC analysis on chiral stationary phase, using Chiracel OD-H as columns with hexane/*i*PrOH mixtures as a mobile phase and UV detection at 254 nm.

To test the recyclability of Pd@IO-DTPA-DNA catalyst, after each cycle catalyst was separated by using an external magnet, washed twice with 10 mL water followed by 10 ml Ethyl acetate and dried in an oven at 100°C for 5 h. The recovered catalyst was further used for the next cycle of reaction.

6.2.6. General procedure for the *p*-Nitrophenol reduction reaction using Pd@IO-DTPA-DNA catalyst

25 mg/L of the *p*-NP solution was prepared with conductivity water. In a 100 ml conical flask, 50 ml of the 25 ppm *p*-NP solution, 7 mg of NaBH₄ and 1 mg of the Pd@IO-DTPA-DNA catalysts were added. The solutions were mixed by shaking before each measurement. The reduction reaction was monitored using UV–Vis absorption spectrophotometer within a range of 200 to 600 nm at different time intervals. A color change from bright yellow to colorless of the solution was observed.

The reusability of the catalyst was tested by a scale-up experiment with 10 mg of catalyst and maintaining the same ratio of catalyst/*p*-NP. The catalyst was separated by hand held magnet, and washed twice in 20 mL conductivity water and 1 ml Acetone, and then placed in a drying oven to dry for 5 h (at 100 °C), and then used for the next run.

6.2.7. Characterization techniques and methods of analysis of synthesized nanosystems (IO-DTPA-DNA and Pd@IO-DTPA-DNA)

The structural and morphological properties of IO-DTPA-DNA and Pd@IO-DTPA-DNA were analyzed by, UV-Vis, IR, XRD, SEM, EDX, VSM, HRTEM, XPS, HRTEM, TG-DTA and XANES techniques.

GC-MS spectra of crude products obtained after coupling reaction and NMR Spectra of column purified biphenyl products were recorded in CDCl₃ solvent using procedure described in chapter 3.

Specific optical rotation (SOR)

Biaryl derivatives obtained from Suzuki coupling reaction were weighed and dissolved in CHCl_3 . This solution was kept at 25 °C for 10-15 min. Prepared solutions were filled in cuvette and the data was recorded at 20 °C by using Jasco p-2000 instrument using Na lamp with 589 nm as a source.

High Performance Liquid Chromatography (HPLC) analysis

HPLC analysis were performed by dissolving Samples (Biaryl derivatives) in n-Hexane in non-polar solvent system (n-Hexane:Isopropanol (99:1)). Daicel OJ-H column was used to perform chiral HPLC (Thermo fisher scientific dionex ultimate 3000) analysis for the separation of enantiomers.

6.3. Result and discussion

6.3.1. Characterization of IO-DTPA-DNA and Pd@ IO-DTPA-DNA

6.3.1.1. FTIR spectra

Comparative FTIR spectra of IO-DTPA, IO-DTPA-DNA and Pd@IO-DTPA-DNA are shown in Figure 6.1. Characteristic peaks of DTPA were present in the FT-IR spectra of IO-DTPA. The bands observed at 630, 560 cm^{-1} in IO-DTPA, at 637, 581 cm^{-1} in IO-DTPA-DNA, and at 634, 571 cm^{-1} in Pd@IO-DTPA-DNA corresponded to the Fe-O stretching vibration (MTh-O-MOh of the tetrahedral and octahedral sites). Further the band at 437 cm^{-1} may be attributed to the Fe-O stretching mode of octahedral sites of maghemite.

The presence of new IR bands in IO-DTPA-DNA and Pd@IO-DTPA-DNA originating from the vibration of chemical bonds in the CT-DNA structure clearly confirmed the successful capping of CT-DNA on IO-DTPA. Apart from the peaks in the 3000– 3500 cm^{-1} range which belong to N-H and C-H stretching, the major peaks at 1626 cm^{-1} (C=O stretching Thymine and Guanine), 1657 cm^{-1} (C=N), and 1540 cm^{-1} (C=C) of DNA nucleobases and peaks at 1226 cm^{-1} (anti symmetric stretching vibration of PO_2^-), 974 cm^{-1} (C-C and C-O of deoxyribose skeletal (backbone) stretching) were observed (Kandathil et al., 2020; Santhiya et al., 2013; Sarioglu et al., 2014).

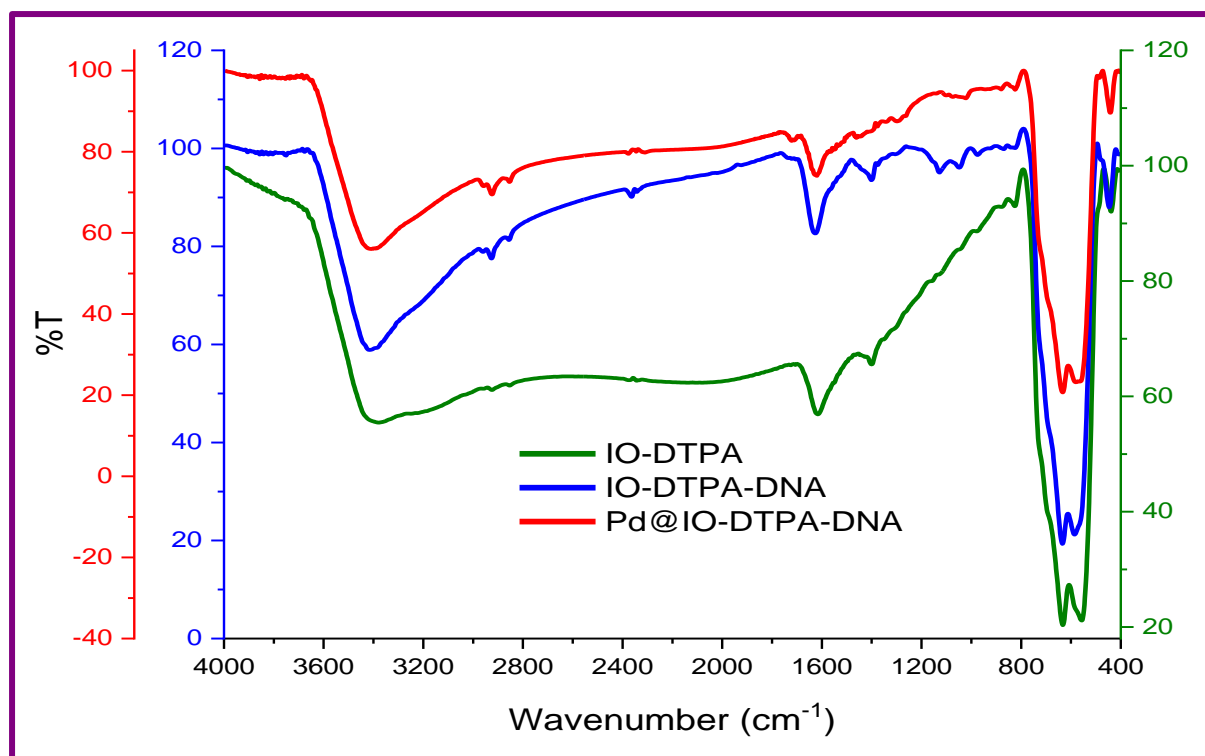


Figure 6.1 Overlay IR spectra of IO-DTPA, IO-DTPA-DNA and Pd@IO-DTPA-DNA

The successful incorporation of CT-DNA onto IO-DTPA can be understood from Figure 6.1, wherein the peaks corresponding to both DNA and IO-DTPA were present with a slight shift in the wave numbers. Again, after the immobilization of Pd on IO-DTPA-DNA, a peak shift was observed when compared with the peaks of IO-DTPA-DNA which could be due to the interaction of Pd with IO-DTPA-DNA. For instance, the peak at 1626 cm^{-1} was shifted to 1621 cm^{-1} . Another significant difference was the decrease in intensity of peak at 1045 cm^{-1} after immobilization of Pd which can be attributed to the interaction of phosphate groups with Pd nanoparticles.

6.3.1.2. ICP-MS and SEM-EDX and HRTEM

ICP-MS elemental analysis shows that the amounts of Pd and Fe are 0.45 and 55.12 wt% respectively. Figure 6.2(A & E) present the SEM micrographs of IO-DTPA-DNA and Pd@IO-DTPA-DNA.

The particles were spherical in shape and the size distribution of the particles is in nanometre range. Furthermore, the EDX results (Figure 6.2(B&F)) confirmed the presence of Fe, P, O, C and N in IO-DTPA-DNA and Fe, P, O, C, N and Pd in Pd@IO-DTPA-DNA. The EDX mapping of Pd@IO-DTPA-DNA indicated uniform dispersion of palladium (2.62 wt%) and on IO-DTPA-DNA (0.68 at%).

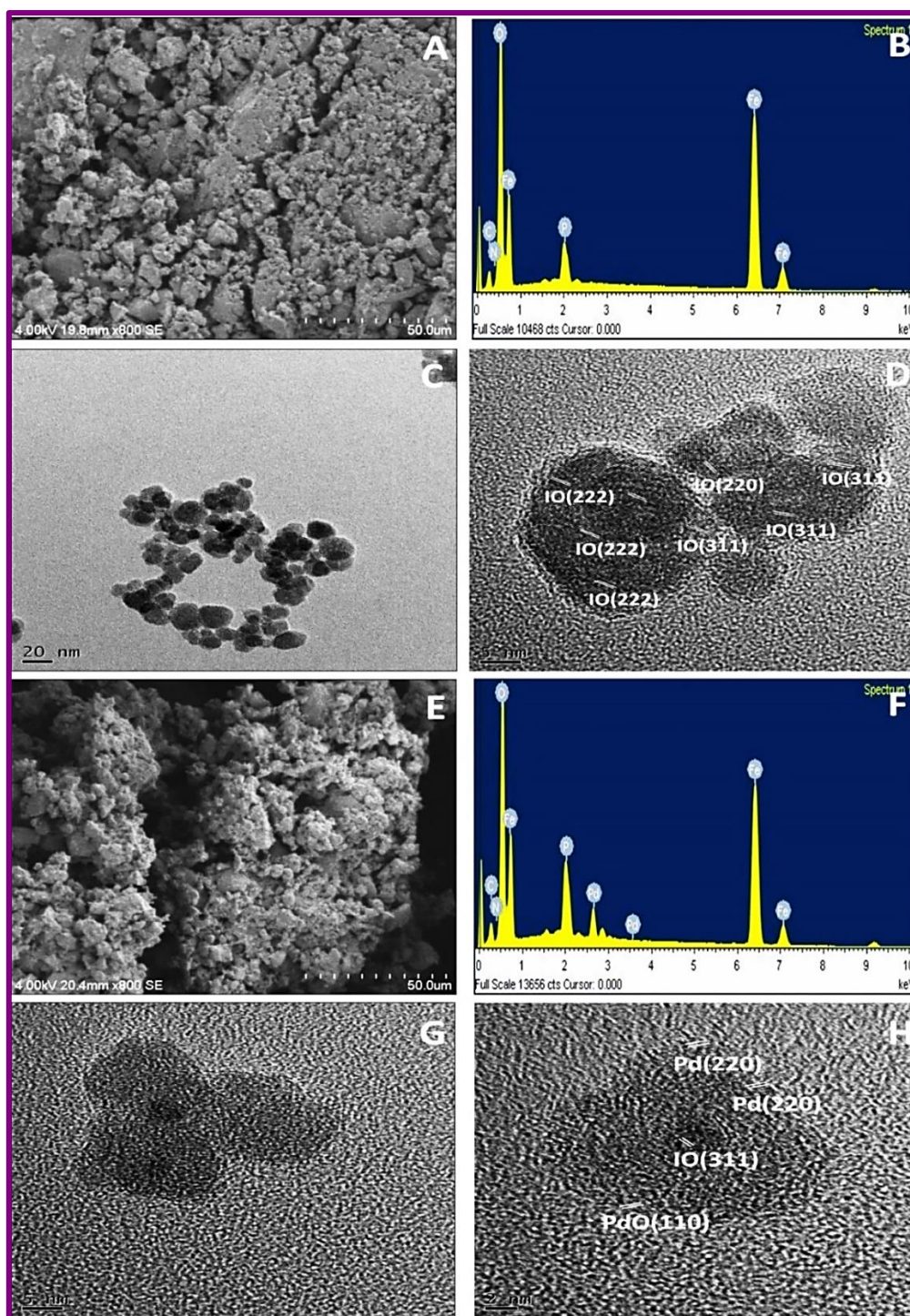


Figure 6.2: (A) SEM image of IO-DTPA-DNA, (B)EDS data of IO-DTPA-DNA, (C) TEM image of IO-DTPA-DNA, (D) HRTEM image of IO-DTPA-DNA, (E) SEM image of Pd@IO-DTPA-DNA, (F)EDS data of Pd@IO-DTPA-DNA, (G) TEM image of Pd@IO-DTPA-DNA, (H) HRTEM image of Pd@IO-DTPA-DNA

Additionally, HRTEM and (SAED) analysis on the obtained nanosystems was performed. As shown in Figure 6.2(C), the size of the synthesized magnetic particles IO-DTPA-DNA ranged

from 5-17 nm. The magnetic nanoparticles with near sphere-shaped morphology were produced.

Micrographs depicted of Pd@IO-DTPA-DNA in Figure 6.2(G&H) clearly reveal that, it consisted of core shell like structure with particle size ranging from 6-18 nm. Figure 6.2(H) depicts the well dispersed Pd NPs grown on the IO-DTPA-DNA nanoparticles support. Regular fringes were clearly observed in the nanoparticle Pd@IO-DTPA-DNA with a spacing of 0.25 nm, 0.265 nm and 0.301 indicating (222), (311), (220) planes of Fe_3O_4 respectively (Predoi et al., 2010), 0.21 nm (220) plane of Pd nanocrystals and 0.245 nm (110) plane of PdO (Vats et al., 2016).

6.3.1.3. XPS analysis

The IO-DTPA-DNA (Figure 6.3) and Pd@IO-DTPA-DNA (Figure 6.4) were further evaluated by X-ray photoelectron spectroscopy (XPS) to obtain the spin states and bonding information of the samples.

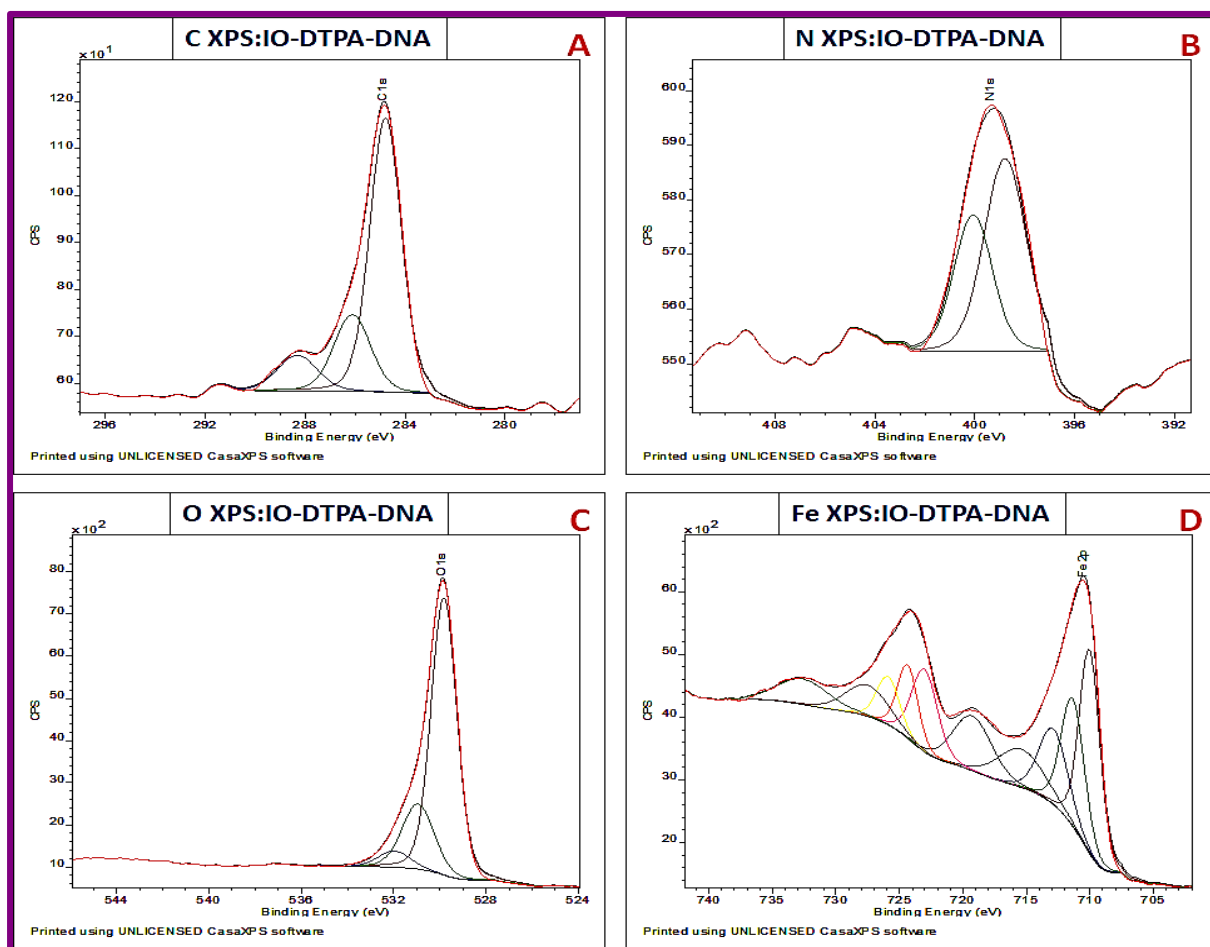


Figure 6.3: C, N, O, Fe XPS spectra of IO-DTPA-DNA

C 1s spectra of IO-DTPA-DNA were de-convoluted into representative chemical groups of C-C/C-H, C-N, C=O/COOH which emerged at binding energies of 284.79, 286.12, and 288.32 eV respectively (Figure 6.3 A). O 1s XPS spectra of IO-DTPA-DNA exhibited peaks at 529.82, 530.94, 531.97 eV that can be attributed to C=O, P-O and COOH bonds (Figure 6.3C). The N1s peak at 398.79 and 400.07 eV represented C=N and -N-C-O bond respectively (Figure 6.3B). The P XPS (Figure 6.A1) peaks around 132 eV and 133 eV, were attributed to P 2p_{3/2} and P 2p_{1/2}, respectively, which is characteristic of PO₄³⁻ of DNA (Mart et al., 2018). The deconvoluted Fe2p XPS spectra of IO-DTPA-DNA (Figure 6.3D) exhibited a peak at 710.03 eV attributed to octahedral Fe³⁺ 2p 3/2 of γ -Fe₂O₃ and α -Fe₂O₃ while the satellite peak of Fe³⁺ was observed at 719.25 eV. Peak at 723.03 eV attributed to Fe2p_{1/2} indicated the presence of Fe³⁺. The peak at 711.36 and 712.89 eV can be attributed to octahedral and tetrahedral Fe³⁺ in Fe₃O₄.

Similarly, for Pd@IO-DTPA-DNA, (Figure 6.4) peaks attributed to C-C/C-H, C-N, C=O/COOH were found at binding energies of 284.8, 286.18, 288.68 eV respectively (Figure 6.4A). The O 1s core spectra were de-convoluted into chemical species of C=O, P-O and COOH bonds, which emerged at 529.79, 531.10, 532.29 eV respectively (Figure 6.4C).

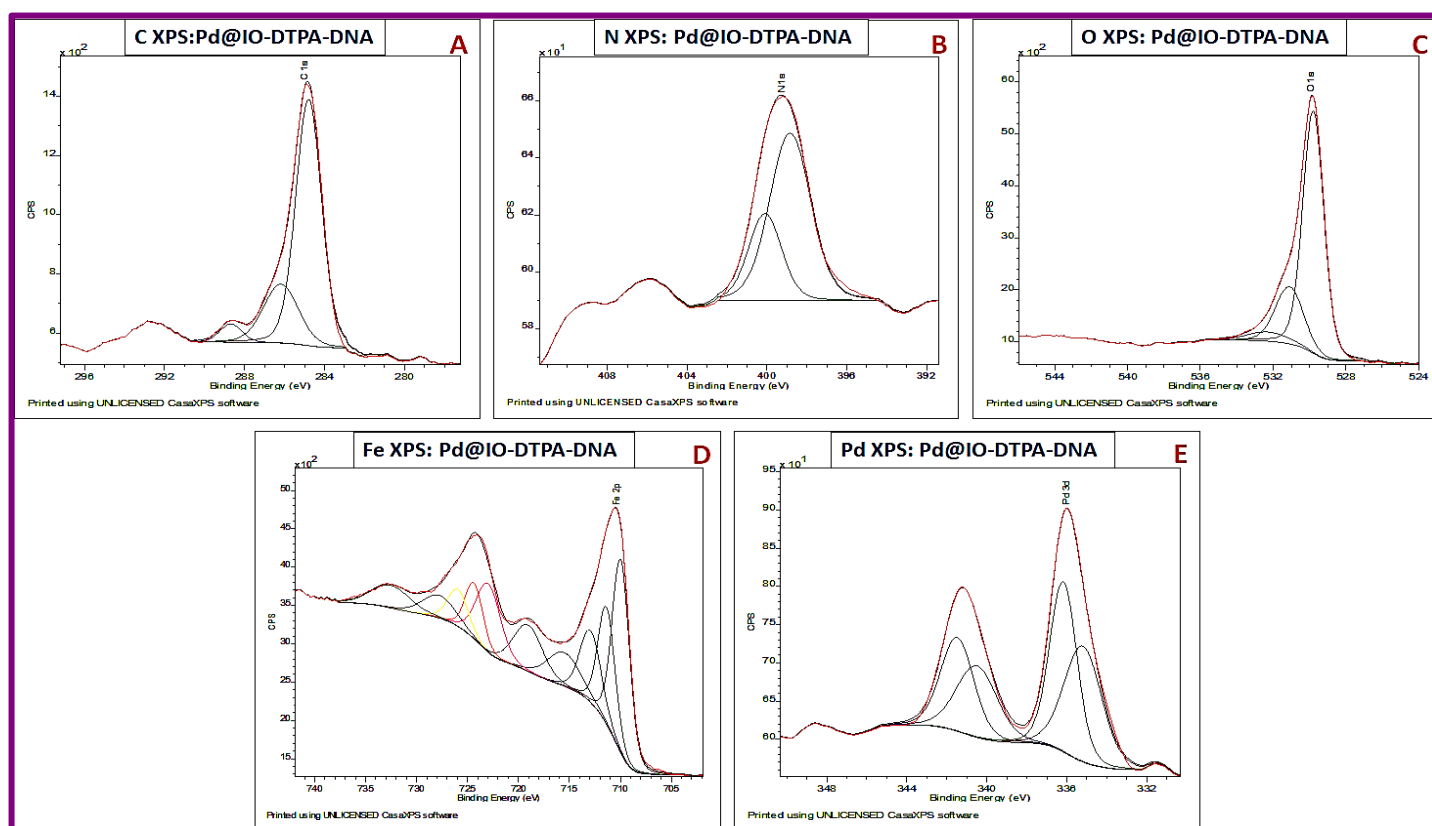


Figure 6.4: C, N, O, Fe, Pd XPS spectra of Pd@IO-DTPA-DNA

P XPS (Figure 6.A1) exhibited a single peak at ~132 eV attributed to P 2p_{3/2} and P 2p_{1/2} respectively which is characteristic of phosphate group of DNA clearly indicating that combination of Pd with DNA (Qu et al., 2012). The deconvoluted N1s peak (Figure 6.4B) at 398.84 and 400.10 eV represented C=N and -N-C-O bond respectively (Mart et al., 2018). Fe2p XPS spectra of Pd@IO-DTPA-DNA (Figure 6.4D) showed deconvoluted peaks at 709.97 and 722.97 eV assigned to octahedral Fe³⁺2p_{3/2} and Fe³⁺2p_{1/2} of γ -Fe₂O₃ and α -Fe₂O₃ respectively with a spin orbit splitting of 13 eV. The peak at 712.94 eV can be attributed to tetrahedral Fe³⁺ in Fe₃O₄. The peaks at binding energies of 335.2 eV and 340.5 eV were assigned to Pd(0) 3d_{5/2} and 3d_{3/2} orbitals with a spin orbit splitting of 5.3eV. The Pd3d_{5/2} peak observed at 336.18eV was attributed to Pd²⁺ (Chakraborty et al., 2019) (Figure 6.4E).

6.3.1.4. PXRD Spectra

The crystallinity and phase of the nanocatalysts (IO-DTPA-DNA and Pd@IO-DTPA-DNA) were determined using X-ray powder diffraction (XRD) analysis (Figure 6.5A). The XRD of IO-DTPA-DNA shows a cubic spinel structure with an average crystallite size of 12.86 nm with peaks observed at 30.15°, 35.5°, 43.2°, 53.6°, 57.27°, 62.98° and 74.38° attributed to (220), (311), (400), (422), (511), (440) and (533) crystal faces of Fe₃O₄ spinel structure in IO-DTPA-DNA (Predoi et al., 2010). The crystallite size was calculated to be 12.86 nm.

Besides the characteristic peaks of iron oxide in Pd@IO-DTPA-DNA, additional weak peaks were observed at 39.96°, 47.1° and 69.4° attributed to (111), (200) and (220) crystalline planes of face centered Pd nanoparticles in good agreement with (JCPDS file number 46-1043) (Vats et al., 2016). Further, diffraction peaks of PdO corresponding to (112) and (200) Bragg planes were also observed (Ganji et al., 2013). The crystallite size of Pd@IO-DTPA-DNA was found to be 13.3 nm.

The crystallite sizes obtained for Pd@IO-DTPA-DNA and IO-DTPA-DNA were in good agreement with sizes estimated from HRTEM images (Blanco-Gutiérrez et al., 2019).

6.3.1.5. XANES analysis

Figure 6.5B displays the Fe K-edge XANES spectra obtained from Pd@IO-DTPA-DNA catalyst. The result of XANES analysis showed that the chemical state of iron in the material is similar to the chemical state of iron in γ -Fe₂O₃ (Baumgartner et al., 2013).

The Pd K-edge XANES spectra (Figure 6.5C) reveals that a peak at 24373.07 eV is indicative of PdO and hump at 24358.87 eV suggested the presence of metallic Pd (Keating et al., 2013).

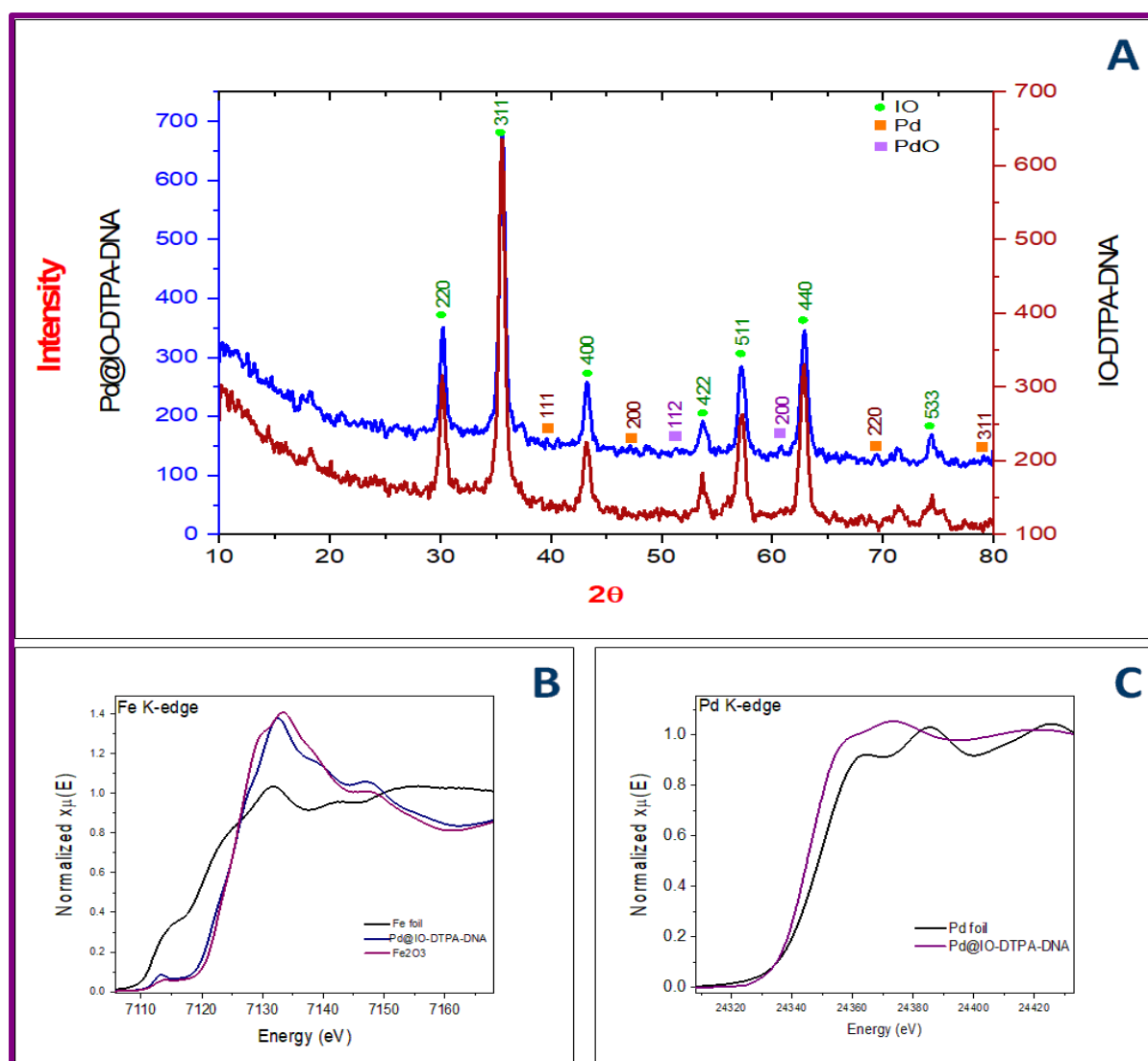


Figure 6.5: (A) overlay XRD spectra of IO-DTPA-DNA and Pd@IO-DTPA-DNA, (B) Fe K edge XANES of Pd@IO-DTPA-DNA, (C) Pd K edge XANES spectra of Pd@IO-DTPA-DNA

6.3.1.6. TG-DTA analysis

The thermal properties of IO-DTPA-DNA and Pd@IO-DTPA-DNA were investigated by TGA and are shown in Figure 6.6(A&B) respectively in the temperature range 30 to 700 °C. The thermogram of IO-DTPA-DNA and Pd@IO-DTPA-DNA demonstrated mainly 4 stages of weight loss. The weight losses observed upto ~100 °C was allocated to the adsorbed (surface) water (3.5% in IO-DTPA-DNA and 3.4% in Pd@IO-DTPA-DNA). The weight loss at ~100-250 °C is attributed to the bound water (3.0% in IO-DTPA-DNA and 3.4% in Pd@IO-DTPA-DNA). Weight loss depicted at ~250-700 °C is associated to the decomposition of the capped DTPA & DNA on the surface of magnetic nanoparticle (3.3% in IO-DTPA-DNA and 5.9% in Pd@IO-DTPA-DNA).

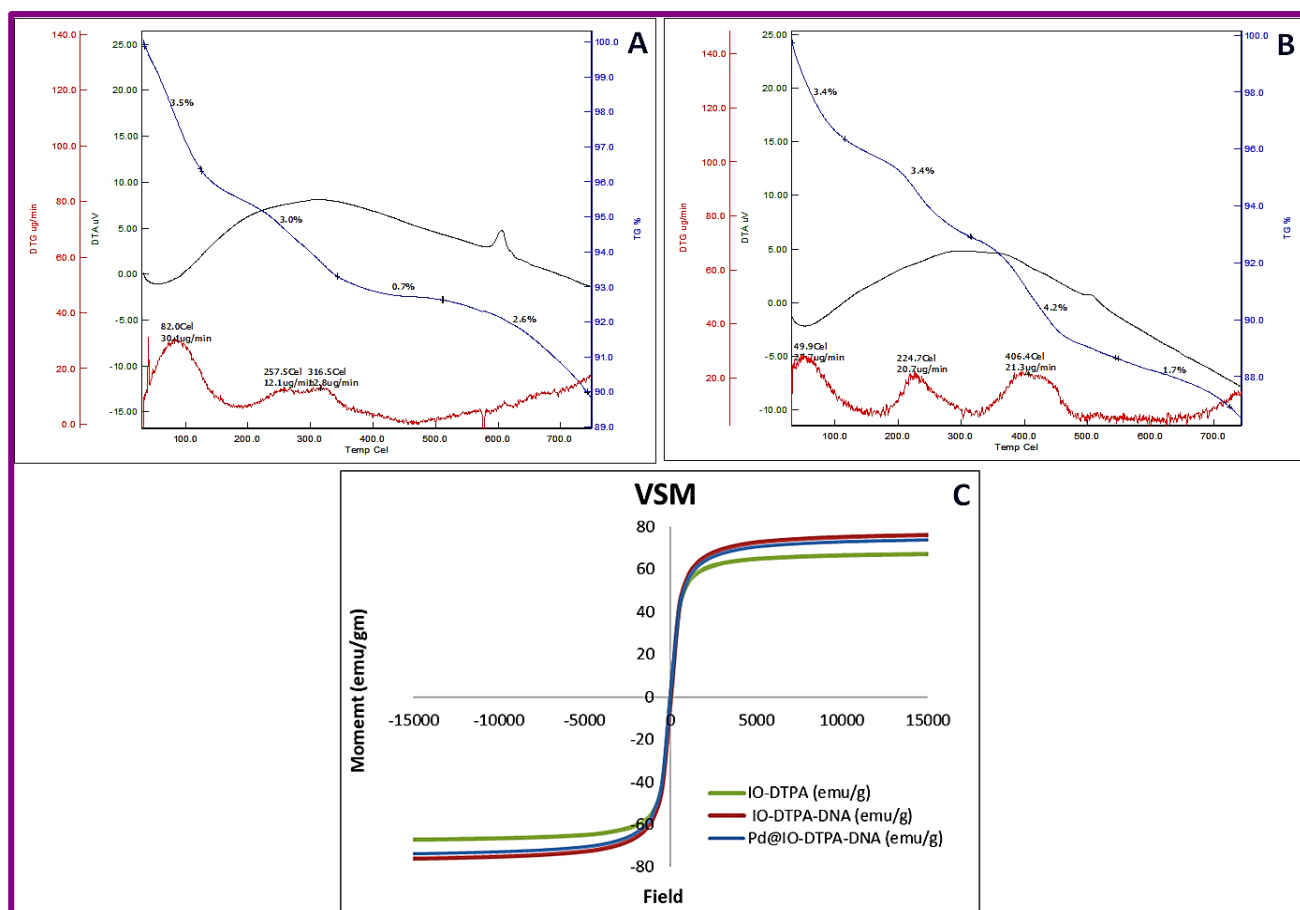


Figure 6.6: (A) Thermogram of IO-DTPA-DNA, (B) Thermogram of Pd@IO-DTPA-DNA, (C) VSM spectra of IO-DTPA-DNA and Pd@IO-DTPA-DNA

6.3.1.7. VSM analysis

Vibrating sample magnetometer (VSM) studies confirmed the superparamagnetic behaviour of IO-DTPA, IO-DTPA-DNA and Pd@IO-DTPA-DNA as VSM spectra did not show hysteresis loop (Figure 6.6C). The magnetization curve in Figure 6.6C, indicated saturation magnetization of IO-DTPA-DNA to be 76.001 emu/g. Magnetic response was decreased to 73.92 emu/g after immobilization of nonmagnetic Pd on IO-DTPA-DNA (Lara & José G. Carriazo, 2019). Absence of hysteresis confirmed the superparamagnetic behaviour of both the nanosystems. Furthermore, the catalyst could be easily separated by magnet and can be uniformly dispersed in solution again after the magnetic separation due to its superparamagnetism.

6.4. Catalytic performance studies.

6.4.1. Application of magnetic palladium catalysts (Pd@IO-DTPA-DNA) for p-Nitrophenol reduction

Attempt was made to use the Pd@IO-DTPA-DNA as a catalyst for the reduction of p-Nitrophenol (Figure 6.7) at room temperature using Sodium borohydride as a reducing agent. Pale yellow colour of p-NP aqueous solution exhibited absorption peak at 318 nm. After addition of NaBH₄, the color of the solution changed to dark yellow with an absorption maximum at 404 nm due to formation of nitrophenolate ion.

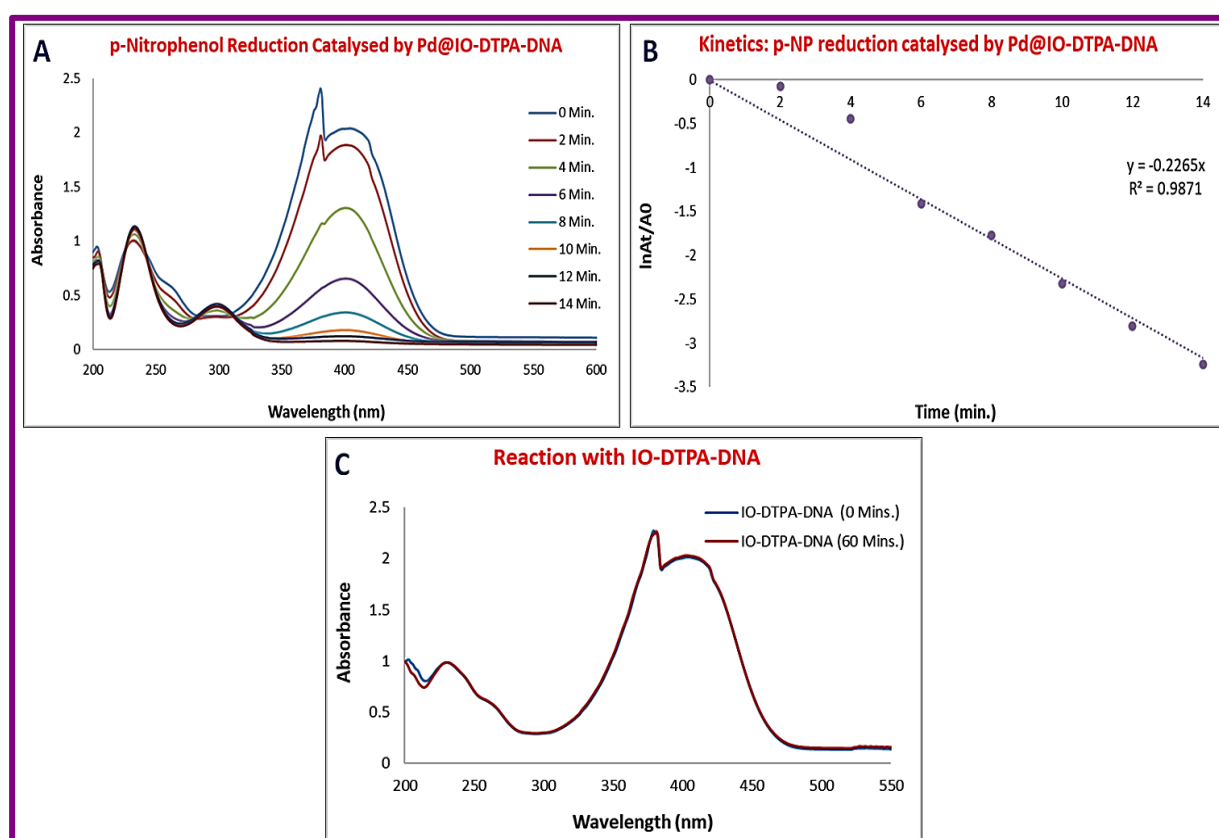


Figure 6.7: (A) Time study of p-NP reduction catalysed by Pd@IO-DTPA-DNA, (B) Kinetics of p-NP reduction catalysed by Pd@IO-DTPA-DNA, (C) p-NP reduction catalysed by IO-DTPA-DNA

The kinetics of the Pd@IO-DTPA-DNA (Figure 6.7B) catalyzed reduction reaction followed pseudo first-order rate. The plot of $\ln(A_t/A_0)$ versus time showed linear relationship and the rate constant, k , was calculated to be 0.2265 min^{-1} .

The Pd@IO-DTPA-DNA catalyst could be readily magnetically recovered. After each run, it was dried and used for the further reaction. Pd@IO-DTPA-DNA showed high recyclability up to twenty-five times for p-NP reduction. After 28th cycle, reaction time had increased to 20 min. and remained the same upto 32 cycles. In order to understand the role of palladium in the catalyst a blank reaction was performed with IO-DTPA-DNA. The reaction did not proceed even when continued till 60 minutes (Figure 6.7C),

6.4.2. Application of magnetic palladium catalysts (Pd@IO-DTPA-DNA) for Suzuki coupling reaction

The Suzuki-Miyaura coupling, one of the most efficient coupling reactions even to form axially chiral biaryls, was used to evaluate the catalytic activity of Pd@IO-DTPA-DNA. Thus, the coupling reaction between aryl halide and aryl boronic acid was examined. Initially, we have chosen the coupling reaction of Iodobenzene (1.59 mmol) and phenylboronic acid (1.59 mmol) as model coupling reaction for the optimization of reaction conditions under heating and water was used as a solvent.

Several solvent systems such as Ethanol, Isopropanol, DMF, toluene, and tetrahydrofuran (THF), H₂O/Ethanol and H₂O/Isopropanol were tested. A high yield was achieved with H₂O, H₂O/Ethanol and H₂O/Isopropanol as solvent (Figure 6.8A). It was found that the least yield was obtained when THF and DMF was utilized as the solvent.

For the optimization of base, several bases such as Et₃N, NaOH, KOH, Na₂CO₃, K₂CO₃, etc. (Figure 6.8B) were used. Study with different bases indicated that they have remarkable effect on the yields of the product. KOH, NaOH and K₂CO₃ gave high yields. Lowest yield was observed with Triethyl amine (TEA). Complete conversion was obtained even when 0.75 equivalent of K₂CO₃ was used in the reaction. (Figure 6.8C) When base was not added to the reaction medium the reaction did not proceed to completion even after 15 h. Investigation of base amount was done with bromobenzene and chlorobenzene as starting materials. For both the starting materials 1 equivalent K₂CO₃ was required for the completion of the reaction. Therefore, 1 equivalent of K₂CO₃ was used in the further reactions.

The effect of temperature in the Suzuki coupling catalytic system was studied with Pd@IO-DTPA-DNA. Reactions with Iodobenzene and Phenylboronic acid conducted at room temperature (30 °C), 40°C, 60°C, 80°C and 100°C were most efficient in water and gave 100% yield at all the temperature (Table 6.A7, entries 13, Figure 6.A6). The optimum reaction

temperature for the catalytic conversion was found to be room temperature. There was no improvement in the yield as well as in reaction time with increase in temperature but the improvement in yield was observed for the other Aryl halides and highest yield was observed at 100 °C. Therefore, all catalytic studies with Pd@IO-DTPA-DNA were carried out at 100 °C. (Table 6.1).

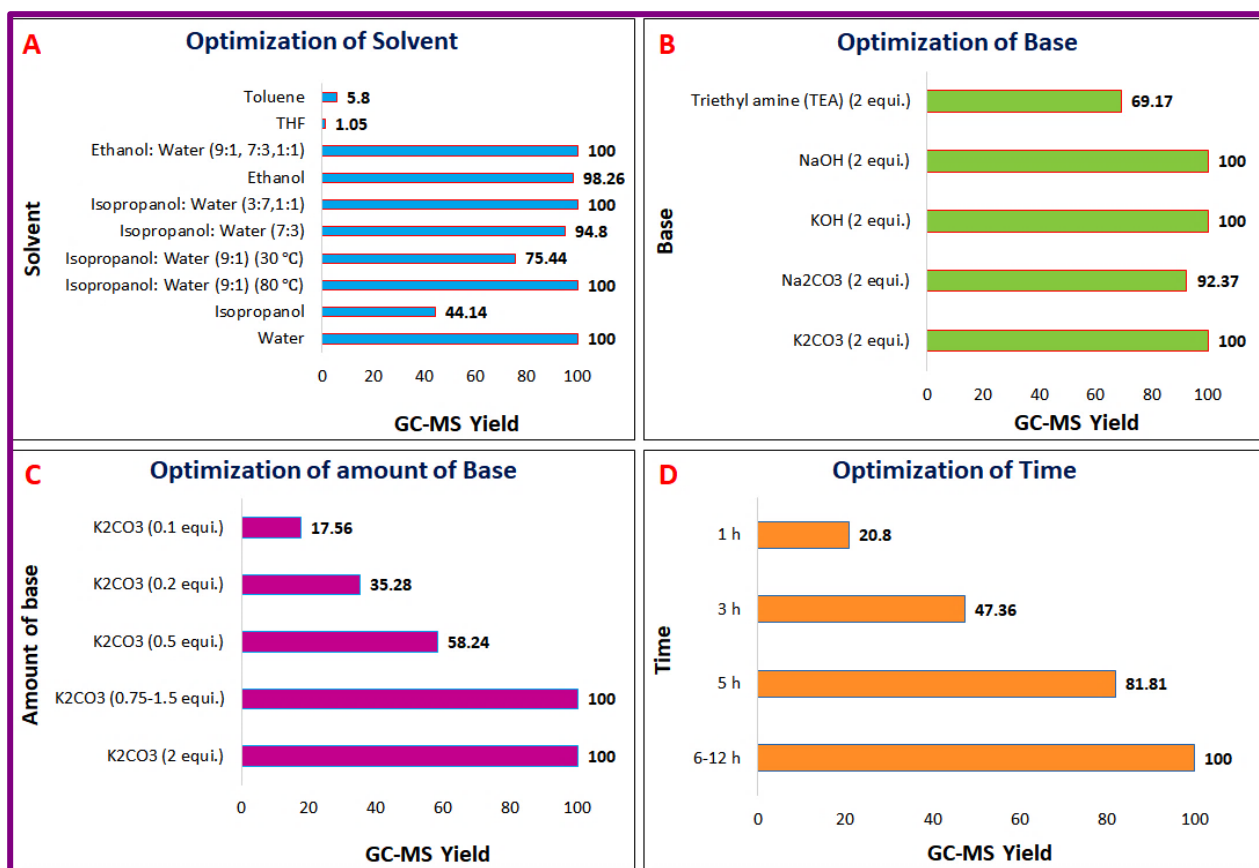


Figure 6.8: Optimization of reaction condition for Suzuki coupling reaction; **Reaction condition:** Iodobenzene (1.59 mmol), Phenylboronic acid (1.59 mmol); Base-K₂CO₃, Water (solvent) 10ml, Catalyst (1 mg), TLC(*n*-Hexane), GC-MS (HPLC grade chloroform), Yields were obtained by GC-MS analysis.

To optimize the amount of catalyst Pd@IO-DTPA-DNA, the reaction of Iodobenzene (1.59 mmol) with Phenylboronic acid (1.59 mmol) in the H₂O solvent system at 100 °C was considered. Therefore, the optimum amount of the catalyst was 0.00427 mol % Pd (Table 6.A7 entry 1). Increasing the catalyst loading did not improve the yield of the product significantly. Control experiments showed that no product formation took place in the absence of Pd@IO-DTPA-DNA and in presence of IO-DTPA-DNA in aqueous medium.

It was observed that quantitative yields were obtained with progressive increase of time from 1 to 12 h at 100 °C. Monitoring of the reaction time indicated that the reaction was completed in 6 h from the start of the reaction at 100 °C (Figure 6.8D).

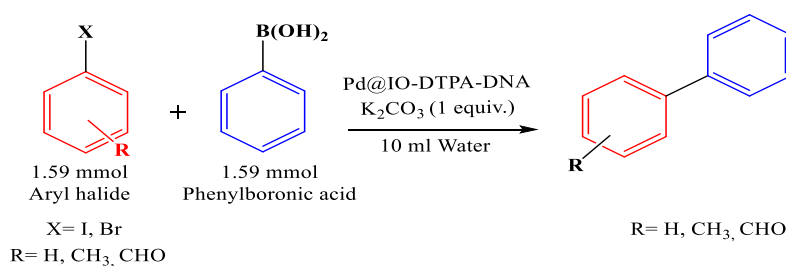
The reaction conditions were systematically optimized and the best result was obtained with 1.59 mmol of Iodobenzene; 1.59 mmol of phenylboronic acid, 0.00427 mol% (1 mg) of catalyst, 1.59 mmol of K₂CO₃ and 10 mL of H₂O at 100 °C for 6 h, which gave an excellent yield with turn over number 23382 and turn over frequency 2922.75 h⁻¹.

After optimization of reaction conditions, the effectiveness of the catalyst was subsequently investigated towards a wide range of substituted aryl halides and arylboronic acids as substrates for Suzuki cross coupling reaction in water as a solvent. In general, all the reactions gave excellent yields of coupling product (Table 6.1).

This study shows that aryl iodides (Table 6.1 entry 1) and aryl bromides (Table 6.1 entry 6) can easily react with phenylboronic acid. However, aryl chloride (Table 6.1 entry 7) reacts slowly with phenylboronic acid. In the oxidative addition step, adding palladium into a C–X bond occurs in the order I > Br > Cl mainly based on the strength of the C–X bond. Considering the above-mentioned reaction protocol, this magnetic catalyst can be applicable to a wide range of aryl halides in all cases. However, aryl iodides containing electron withdrawing group (-CHO) as substrates gave slightly more yields (Table 6.1 entries 4&5) as compared to the electron donating counterpart (-CH₃) (Table 6.1 entries 2&3). Increasing the reaction time further led to formation of biphenyl and cleavage of methyl group from the aromatic ring.

Table 6.1: Suzuki cross-couplings of several aryl halides with arylboronic acids that were investigated using Pd@IO-DTPA-DNA catalysts. at 30 °C, 60 °C and 100 °C

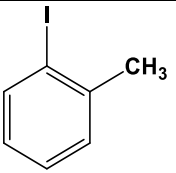
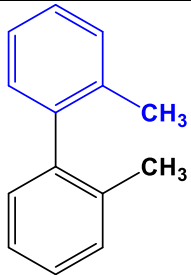
Reaction condition: Aryl halide (1.59 mmol), Phenylboronic acid (1.59 mmol), K₂CO₃ (1.59 mmol), 10 ml water, catalyst dose: 1 mg, TLC (n-hexane), GC-MS (HPLC grade chloroform), Isolated yields based on material isolated (average of two runs)



Sr. No.	X	R	(30 °C), Time (h)	GC-MS Yield (%)	(60 °C), Time (h)	GC-MS Yield (%)	(100 °C), Time (h)	GC-MS Yield (%)	Isolated Yield (%)
1	I	H	8 h	100	8 h	100	6 h.	100	99.99
2	I	p-CH ₃	15 h	56.49	13 h	62.68	13 h	95.86	95.4
3	I	o-CH ₃	16 h	55.37	16 h	61.15	15 h	93.96	93.5
4	I	p-CHO	14 h.	96.82	14 h	100	14 h	100	99.99
5	I	o-CHO	19 h	74.82	18 h	92.49	17 h	98.95	99.99
6	Br	H	12 h	34.80	10 h	91.26	8 h	100	99.99
7	Cl	H	15 h	24.51	12 h	45.67	9 h	100	99.99

Using mono-ortho substituted arylboronic acids afforded products gave good to moderate yields (table 6.2 entries 1-3) but with excellent enantioselectivity (table 6.2 entry 3). An aryl halide with a bulkier substituent at the 2-position of the naphthalene would lead to higher selectivity. The use of 1-bromo-2 methyl naphthalene with o-tolylboronic acid was investigated. The methyl group set close to the Ar–Ar' bond generates more steric hindrance in the transition state. This reaction required more time (48 h) to reach high yield (table 6.2 entry 3) (Benhamou et al., 2014).

Asymmetric Suzuki coupling reaction catalysed by Pd@IO-DTPA-DNA

Sr. no.	Aryl halide	product	Temperature (°C), Time (hrs.)	GC-MS yield (%)	Column yield (%)	ee	SOR
1			100 °C, 20 h	93.24	92.8	-	+3.224

2			100 °C, 24 h	93.29	93.1	-	+6.916
3			100 °C, 48 h	71.67	70.5	99.8	+3.79

Table 6.2: Asymmetric Suzuki cross-couplings of several aryl halides with arylboronic acids that were investigated using Pd@IO-DTPA-DNA catalysts. **Reaction condition:** Aryl halide (1.59 mmol), o-tolylboronic acid (1.59 mmol), K₂CO₃ (1.59 mmol), 10 ml water, catalyst dose: 1 mg, TLC (n-hexane), GC-MS (HPLC grade chloroform), Isolated yields based on material isolated (average of two runs)

To obtain information about the presence of leached palladium in reaction system hot filtration test was performed. The reaction of Iodobenzene with phenylboronic acid was stopped in 3 h at 100 °C, the catalyst was removed from reaction mixture and the reaction was further continued for 10 h. There was no further conversion in the catalyst-free solution. This result points out to the fact that, Pd@IO-DTPA-DNA acted as an effective heterogenous catalyst for the Suzuki coupling reaction at 100 °C in water as solvent (Figure 6.A23).

6.4.3. Recyclability of the catalyst

Encouraged by the good catalytic activity we examined its recyclability in the reaction of Iodobenzene with phenylboronic acid under the above-mentioned optimized conditions. After completion of the reaction the catalyst was separated by magnet from the mixture, washed it with H₂O and ethyl acetate alternatively and finally dried in oven. Then it was reused directly for the next cycle without any further treatment. This experiment showed that Pd@IO-DTPA-DNA can be recycled up to sixteen times without major loss of yield of product and no significant loss of palladium was observed from ICP-MS (Figure 6.9F). After 16th cycle reaction time has increased to 8 h up to 19th cycle which may be due to the palladium loss (1.9%) as evident from leaching study (Figure 6.A24).

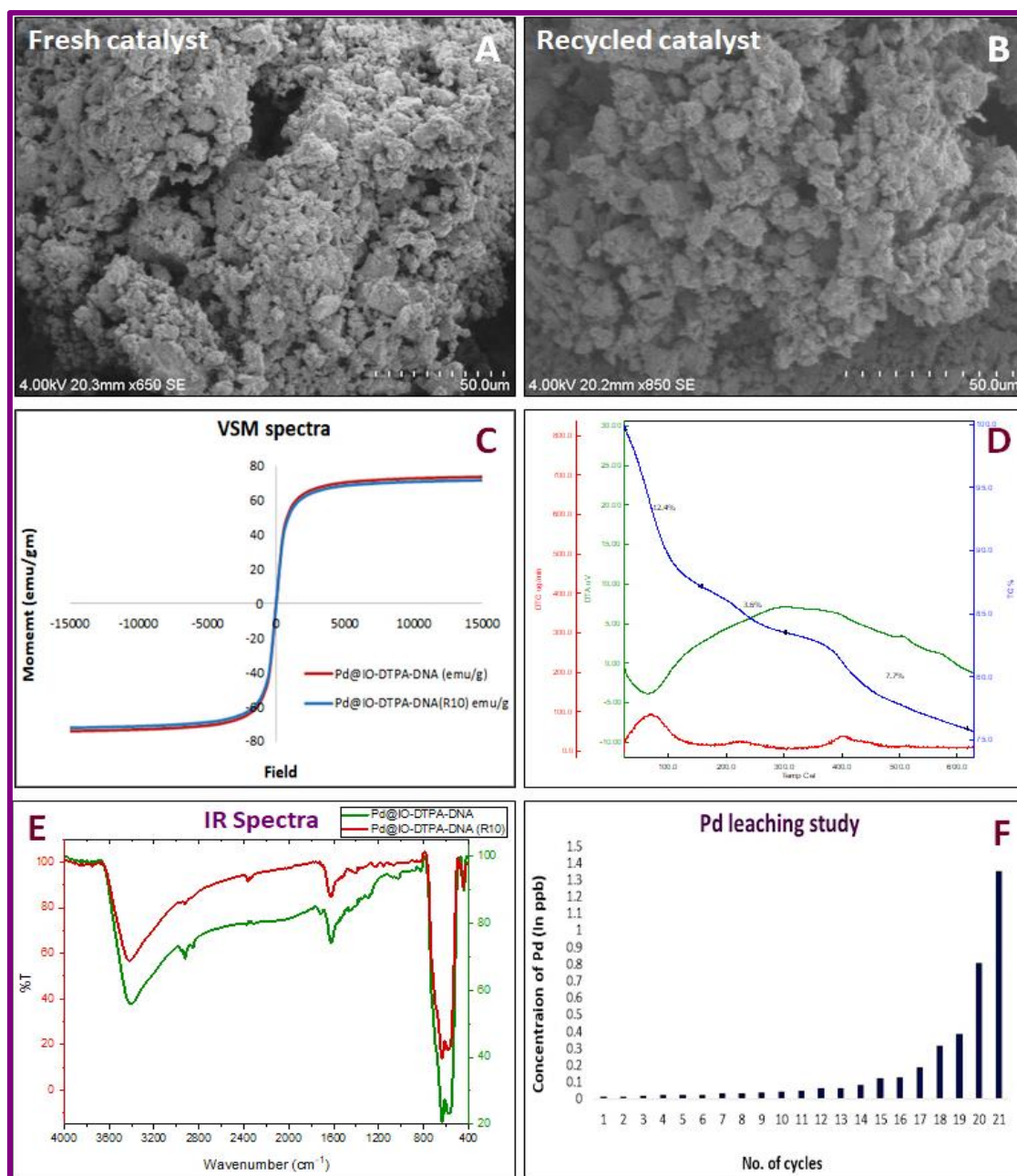


Figure 6.9: (A) SEM image of fresh catalyst, (B) SEM images of Recycled catalyst, (C) VSM spectra of fresh and recycled catalyst, (D) TGA thermogram of Recycled catalyst, (E) IR spectra of fresh and recycled catalyst

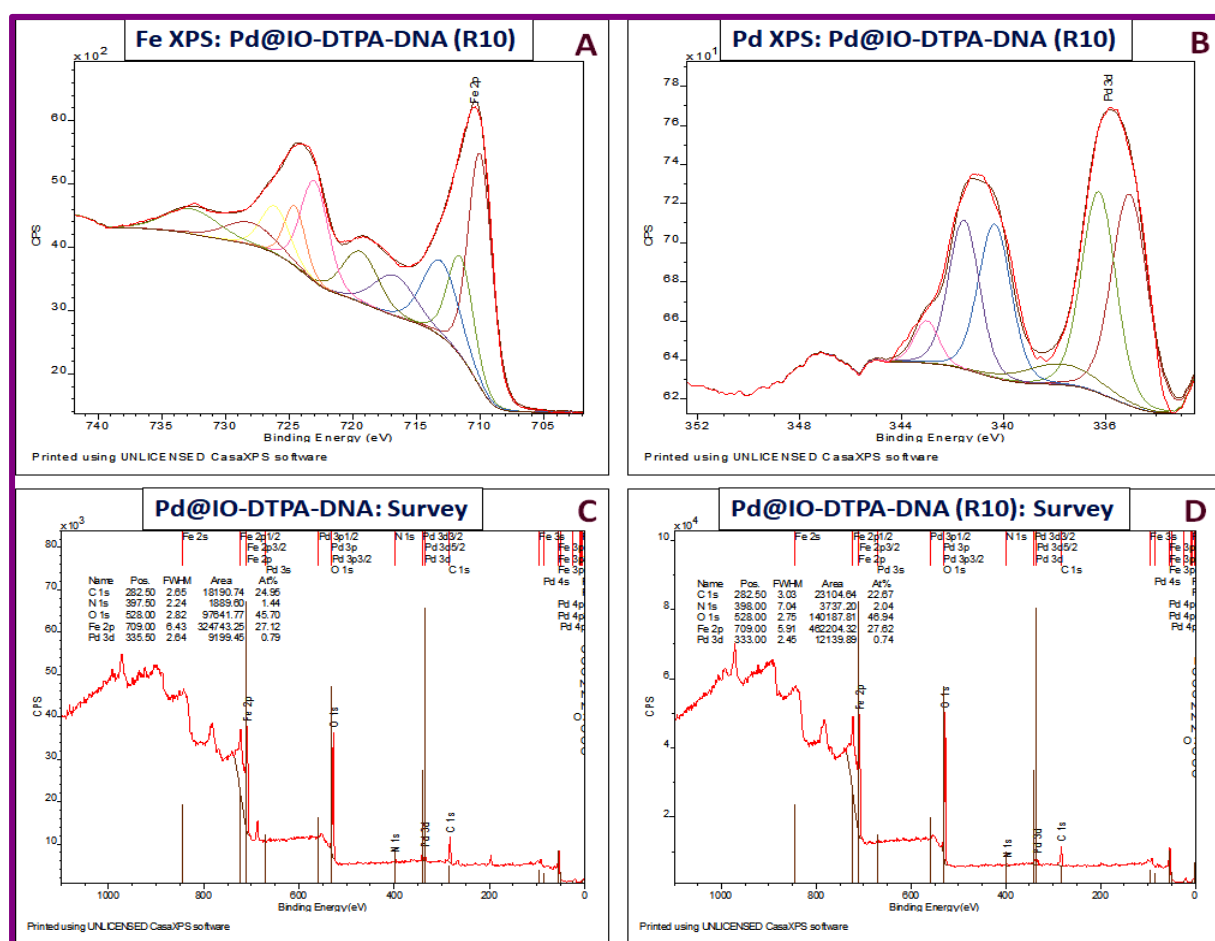
It was found out from GC-MS analysis as well as column purification that 100% conversion was obtained with Pd@IO-DTPA-DNA and 0% with IO-DTPA-DNA where no biphenyl formation was observed.

The SEM image of the recovered catalysts (Figure 6.9 A&B) and after 19th cycles showed well dispersed spherical nanoparticles with practically the same mean diameter, thus no aggregation processes has taken place. The magnetic response of fresh catalyst was 73.92 emu/g which

slightly decreased to 71.99 emu/g. The catalyst could be easily separated by a magnet and could be uniformly dispersed in the reaction system again after the magnetic separation due to its superparamagnetism (Figure 6.9C).

The weight loss observed at ~30-100 °C during TGA-DTA analysis (Figure 6.9D) attributed to the adsorbed water increased from 3.4% in fresh Pd@IO-DTPA-DNA to 12.4 % in recycled catalyst (after 19th cycle). However, the weight loss of 5.9% in fresh Pd@IO-DTPA-DNA at ~250-700 °C associated to decomposition of the of the capped DTPA & DNA increased to 7.7% in recycled catalyst which may be attributed to partial degradation of the protective capping. A total weight loss of about 25% was observed in fresh catalyst and 25.7% in recycled catalyst, suggesting no significant loss in thermal stability. Overlay IR spectra (Figure 6.9E) also exhibited no changes in IR spectra of fresh and recycled catalyst.

The Fe XPS spectra of recycled catalyst (after the 19th reaction cycle) (Figure 6.10A) exhibited the same characteristic peaks as observed in the fresh catalyst (Figure 6.4D).



From Pd XPS studies, changes were observed in the oxidation state of Pd after the recycling process (Figure 6.10B). Pd XPS spectra of fresh catalyst showed Pd3d5/2 peaks at 335.2 and 336.18 eV corresponding to Pd, Pd²⁺, while, recycled catalyst exhibited Pd3d5/2 peaks at 335.04 and 340.34 eV attributed to metallic Pd(0), 336.25 and 341.55 eV corresponding to Pd²⁺ and the peaks at 343.02 and 337.72 eV attributed to PdO due to the exposure of catalyst in Suzuki coupling reaction at 100 °C for 19 cycles. XPS survey spectrum (Figure 6.10 C&D) showed 2% decrease in C content, 0.6% increase in nitrogen, 3% increase in O and 0.05% decrease in Pd content suggesting high stability of the synthesized nanocatalyst. Detailed XPS assignment of the fresh and recycled catalyst are given in Tables 6.A1-6.A5.

6.4. Conclusion

In conclusion, a unique, quick (short reaction time) and efficient method to synthesize DNA based magnetically separable hybrid palladium Nano catalyst has been successfully developed using Calf thymus (ct-DNA). Synthesized catalyst was characterised by various analysis techniques. XPS and HRTEM confirmed that Core shell nanoparticles with size ranging from 6-18 nm containing Pd and Pd²⁺ has formed. After characterization, it was applied for the Suzuki coupling reaction in aqueous system and p-Nitrophenol reduction with a detailed kinetic study. The recyclability of the catalyst was studied. The catalyst was magnetically separable and recyclable upto 19 times for Suzuki coupling reaction and 32 times for p-NP reduction. This makes overall process (fabrication of catalyst and application) scalable and cost efficient. Even after 19 cycles of Suzuki coupling reaction, a very little change was observed in saturation magnetization value (from 73.92 emu/g to 71.99 emu/g). Pd@IO-DTPA-DNA showed better stability, high magnetization values and high recoverability than the DTPA stabilized nanocatalysts (Pd@IO-DTPA and Pd@Ni@IO-DTPA).

6.5. References

- Baumgartner, J., Morin, G., Menguy, N., Perez, T., Widdrat, M., Cosmidis, J., & Faivre, D. (2013). Magnetotactic bacteria form magnetite from a phosphate-rich ferric hydroxide via nanometric ferric (oxyhydr) oxide intermediates. *Proc Natl AcadSci*, 1(20), 14883–14888. <https://doi.org/10.1073/pnas.1307119110>
- Benhamou, L., Besnard, C., & Kündig, E. P. (2014). Chiral PEPPSI Complexes: Synthesis, Characterization, and Application in Asymmetric Suzuki–Miyaura Coupling Reactions. *Organometallics*, 33, 260–266. <https://doi.org/10.1021/om4009982>
- Blanco-Gutiérrez, V., Andrada-Chacón, A., Sánchez-Benítez, J., Urones-Garrote, E., Sáez-

- Puche, R., & Torralvo-Fernández, M. J. (2019). Superparamagnetic Behavior at Room Temperature through Crystal Chemistry Modification and Particle Assembly Formation: Zinc and Nickel Ferrite Systems'. *J. Phys. Chem. C*, *123*, 16973–16981. <https://doi.org/10.1021/acs.jpcc.9b01898>
- Boersma, A. J., Feringa, B. L., & Roelfes, G. (2007). Alfa, Beta-Unsaturated 2-Acyl Imidazoles as a Practical Class of Dienophiles for the DNA-Based Catalytic Asymmetric Diels–Alder Reaction in Water. *Organic Letters*, *9*(18), 3647–3650. <https://doi.org/10.1021/ol7015274>
- Boersma, A. J., Megens, R. P., Feringa, B. L., & Roelfes, G. (2010). DNA-based asymmetric catalysis. *Chem.Soc.Rev.*, *39*, 2083–2092. <https://doi.org/10.1039/b811349c>
- Chakraborty, S., Mruthunjayappa, M. H., Aruchamy, K., Singh, N., Prasad, K., Kalpana, D., Ghosh, D., Kotrappanavar, N. S., & Mondal, D. (2019). Facile Process for Metallizing DNA in a Multitasking Deep Eutectic Solvent for Ecofriendly C–C Coupling Reaction and Nitrobenzene Reduction [Research-article]. *ACS Sustainable Chemistry & Engineering*, *7*, 14225–14235. <https://doi.org/10.1021/acssuschemeng.9b03224>
- Ganji, S., Bukya, P., Vakati, V., Rao, K. S. R., & Burri, D. R. (2013). Highly efficient and expeditious PdO/SBA-15 catalysts for allylic oxidation of cyclohexene to cyclohexenone. *Catalysis Science & Technology*, *3*(409–414). <https://doi.org/10.1039/c2cy20627g>
- Kandathil, V., Kempasiddaiah, M., Nataraj, S. K., Somappa, S. B., & Patil, S. A. (2020). DNA as a bioligand supported on magnetite for grafting palladium nanoparticles for cross-coupling reaction. *Appl. Organometal. Chem.*, *34*(3), e5357. <https://doi.org/10.1002/aoc.5357>
- Keating, J., Sankar, G., Hyde, T. I., Kohara, S., & Ohara, K. (2013). Elucidation of structure and nature of the PdO-Pd transformation using in situ PDF and XAS techniques. *Physical Chemistry Chemical Physics*, *15*(22), 8555–8565. <https://doi.org/10.1039/c3cp50600b>
- Lara, V. N., & José G. Carriazo. (2019). Fe₃O₄-TiO₂ and Fe₃O₄-SiO₂ Core-shell Powders Synthesized from Industrially Processed Magnetite (Fe₃O₄) Microparticles. *Materials Research*, *22*(3), 20180660. <https://doi.org/10.1590/1980-5373-mr-2018-0660>

- Mart, M., Tylus, W., & Trzeciak, A. M. (2018). Pd/DNA as Highly Active and Recyclable Catalyst of Suzuki–Miyaura Coupling. *Catalysts*, 8(11), 552. <https://doi.org/10.3390/catal8110552>
- Predoi, D., Andronescu, E., Radu, M., Munteanu, M. C., & A. DINISCHIOTU. (2010). SYNTHESIS AND CHARACTERIZATION OF BIO-COMPATIBLE MAGHEMITE NANOPARTICLES. *Digest Journal of Nanomaterials and Biostructures*, 5(3), 779–786.
- Qu, K., Wu, L., Ren, J., & Qu, X. (2012). Natural DNA-Modified Graphene/Pd Nanoparticles as Highly Active Catalyst for Formic Acid Electro-Oxidation and for the Suzuki Reaction. *ACS Applied Materials and Interfaces*, 4, 5001–5009. <https://doi.org/10.1021/am301376m>
- Santhiya, D., Alajangi, H. K., Anjum, F., Sevi, M., & Ganguli, M. (2013). Bio-inspired synthesis of microporous bioactive glass-ceramic using CT-DNA as a template. *J. Mater. Chem. B*, 1, 6329–6338. <https://doi.org/10.1039/C3TB21212B>
- Sarioglu, O. F., Tekiner-gursacli, R., Ozdemir, A., & Tekinay, T. (2014). Comparison of Au (III) and Ga (III) Ions ' Binding to Calf Thymus DNA : Spectroscopic Characterization and Thermal Analysis. *Biol Trace Elem Res*, 160(3), 445–452. <https://doi.org/10.1007/s12011-014-0059-8>
- Vats, T., Dutt, S., Kumar, R., & Siril, P. F. (2016). Facile synthesis of pristine nanocomposites with extraordinary catalytic activities using swollen liquid crystals. *Scientific Reports*, 6, 33053. <https://doi.org/10.1038/srep33053>

Appendix

XPS data:

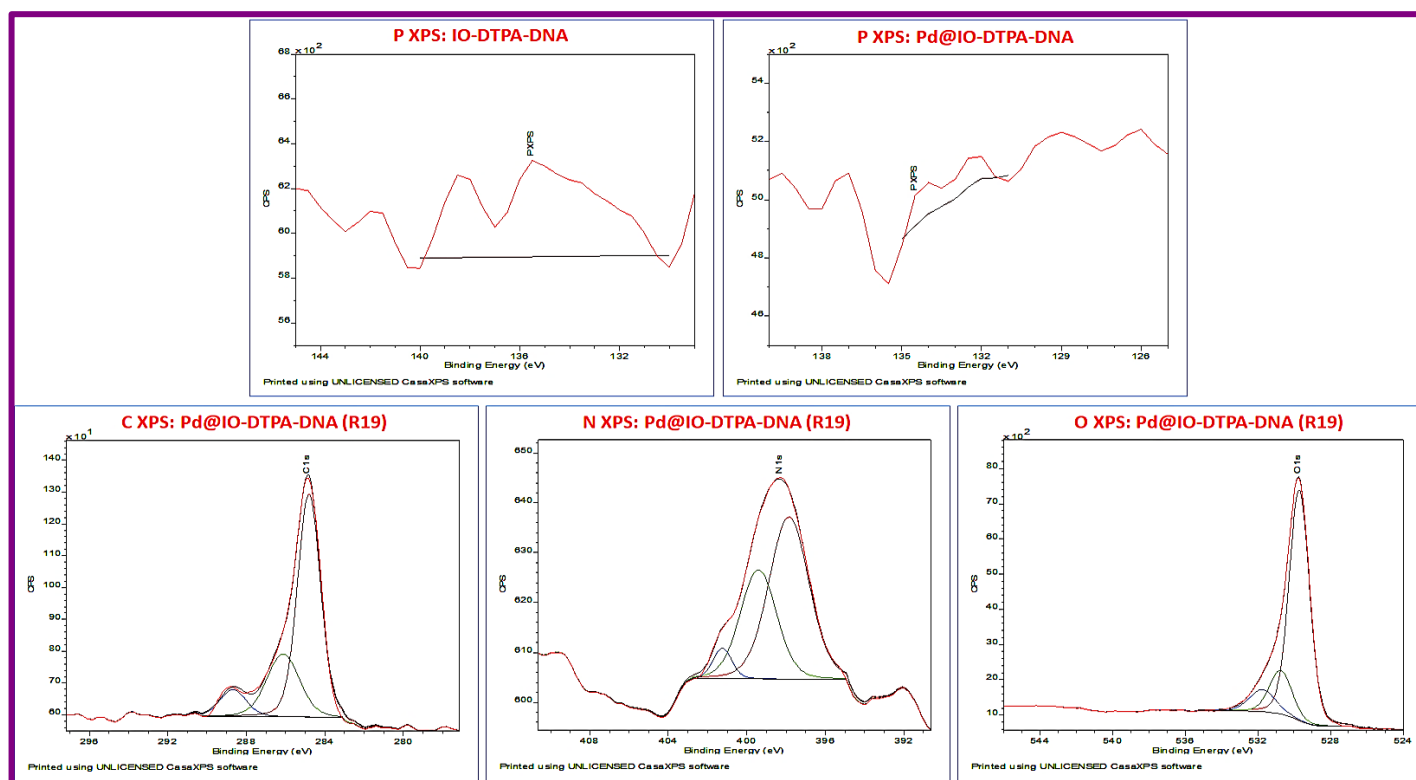


Figure 6.A1: P XPS of IO-DTPA-DNA and Pd@IO-DTPA-DNA & C, N, O XPS spectra of Pd@IO-DTPA-DNA(R19)

Table 6.A1: C1s XPS spectra

Element	IO-DTPA-DNA		Pd@IO-DTPA-DNA		Pd@IO-DTPA-DNA (R19)		Interpretation
	Peak	Area%	peak	Area%	peak	Area%	
C1s	284.79	67.26	284.8	72.03	284.8	65.08	C–C/C–O
C1s	286.12	21.80	286.18	23.40	286.12	25.98	C–N
C1s	288.32	10.94	288.68	4.58	288.68	8.95	O–C–O, O–C=O, N–C=O/–COOH

Table 6.A2: N1s XPS spectra

Element	IO-DTPA-DNA		Pd@IO-DTPA-DNA		Pd@IO-DTPA-DNA (R19)		Interpretation
	peak	Area%	peak	Area%	peak	Area%	
N1s	398.79	60.65	398.84	79.55	397.85	58.84	-C=N
N1s	400.07	39.35	400.10	29.45	399.41	35.92	-N-C-O
N1s					401.25	5.23	

Table 6.A3: O1s XPS spectra

Element	IO-DTPA-DNA		Pd@IO-DTPA-DNA		Pd@IO-DTPA-DNA (R19)		Interpretation
	peak	Area%	peak	Area%	peak	Area%	
O1s	529.82	73.14	529.79	72.06	529.71	74.94	C=O
O1s	530.94	21.48	531.10	22.55	530.74	15.77	P=O
O1s	531.97	5.37	532.29	5.39	531.74	9.28	COOH

Table 6.A4: Fe2p XPS spectra

Element	IO-DTPA-DNA		Pd@IO-DTPA-DNA		Pd@IO-DTPA-DNA (R19)		Interpretation
	peak	Area%	peak	Area%	peak	Area%	
Fe2p3/2	710.03	15.43	709.97	17.58	709.99	18.93	Fe ³⁺ octahedral
Fe2p3/2	711.36	10.87	711.37	10.48	711.55	8.54	Fe ³⁺ octahedral
Fe2p3/2	712.89	7.94	712.94	7.93	713.09	9.12	Fe ³⁺ Tetratahedral
Fe2p3/2	715.40	6.43	715.53	5.81	716.70	5.69	Fe ²⁺ octahedral
Fe2p3/2	719.25	7.71	719.07	7.03	719.39	6.11	Satellite peak of Fe ³⁺ 2p3/2
Fe2p1/2	723.03	14.91	722.97	16.98	722.99	18.29	Fe ³⁺ octahedral

Fe2p1/2	724.36	10.50	724.37	10.13	724.55	8.25	Fe ³⁺ octahedral
Fe2p1/2	725.89	7.67	725.94	7.66	726.09	8.82	Fe ³⁺ Tetratahedral
Fe2p1/2	727.53	9.48	727.77	7.63	728.03	7.44	Fe ²⁺ octahedral
Fe2p1/2	732.63	9.05	732.56	8.76	732.64	8.81	Satellite peak of Fe ³⁺ 2p3/2

Table 6.A5: Pd3d XPS spectra

Element	Pd@IO-DTPA-DNA		Pd@IO-DTPA-DNA (R19)		Interpretation
	peak	Area%	peak	Area%	
Pd3d5/2	335.20	24.41	335.04	24.10	Pd (0)
Pd3d5/2	336.18	26.36	336.25	21.92	Pd (2+)
Pd3d5/2			337.72	4.92	PdO
Pd3d3/2	340.50	23.67	340.34	23.21	Pd (0)
Pd3d3/2	341.48	25.40	341.55	21.12	Pd (2+)
Pd3d3/2			343.02	4.74	PdO

GC MS spectra during optimization of solvent for the reaction between Iodobenzene and phenylboronic acid (Figures 6.A2)

Entry	Solvent	Temp (°C)	Time (h)	GC-MS Yield
1.	Water	100	12	100
2.	Ethanol	80	12	Trace
3.	Isopropanol	80	12	7.8
4.	DMF/DMF	60-100	12	Trace
5.	Toluene	100	12	5.8
6.	Ethanol: Water (9:1, 7:3,1:1)	80	12	100
7.	Isopropanol: Water (9:1)	80	12	100
8.	Isopropanol: Water (9:1)	30	12	75.44
9.	Isopropanol: Water (7:3, 3:7,1:1)	30-80	12	100

Table 6.A6: Optimization of solvent, **Reaction condition:** Iodobenzene (1.59 mmol), Phenylboronic acid (1.59 mmol), catalyst dose: 1 mg, solvent (10 ml), Base- K_2CO_3 (2 equi.), TLC (n-hexane), GC-MS (HPLC grade chloroform)

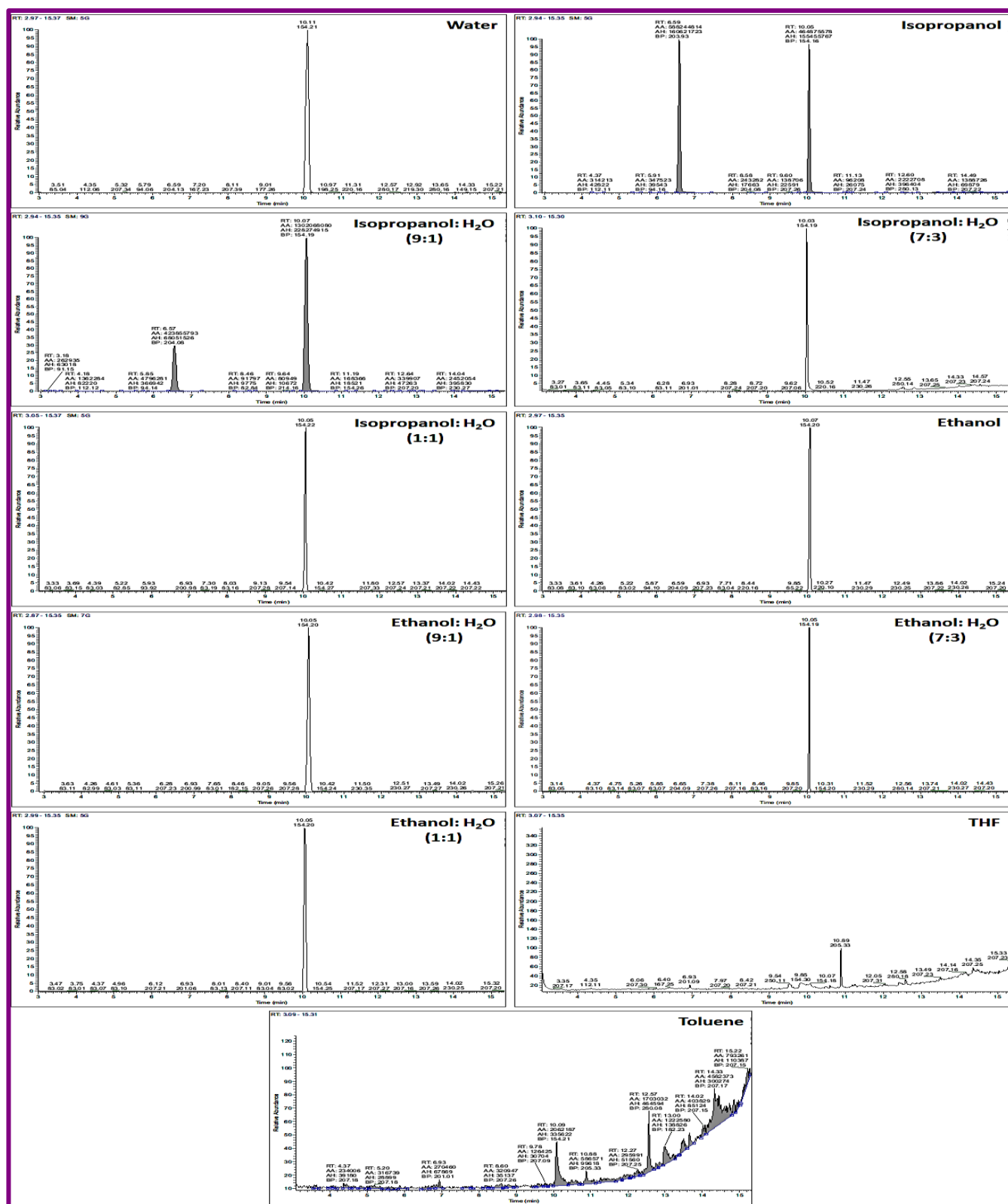


Figure 6.A2: GC-MS spectra of the product for Pd@IO-DTPA-DNA catalysed reaction between iodobenzene and phenylboronic acid performed using K_2CO_3 and in different solvents

Optimization of Base, Temperature and time

Entry	Catalyst amount	Base	Temp (°C)	Time (h)	GC-MS Yield (%)
1.	1-50 mg (0.00427 - 0.021 mol% Pd)	K ₂ CO ₃ (2 equi.)	100	12	100
2.	1 (0.00427 mol% Pd)	K ₂ CO ₃ (2 equi.)	60	12	100
3.	1 (0.00427 mol% Pd)	K ₂ CO ₃ (2 equi.)	30	12	100
4.	1(0.00427 mol% Pd)	Triethyl amine (TEA) (2 equi.)	100	12	69.17
5.	1 mg	Na ₂ CO ₃ (2 equi.)	100	12	92.37
6.	1 mg	KOH (2 equi.)	30-100	12	100
7.	1 mg	NaOH (2 equi.)	30-100	12	100
8.	1 mg	K ₂ CO ₃ (0.75- 1.5 equi.)	30-100	12	100
9.	1 mg	K ₂ CO ₃ (0.5 equi.)	100	12	58.24
10.	1 mg	K ₂ CO ₃ (0.2 equi.)	100	12	35.28
11.	1 mg	K ₂ CO ₃ (0.1 equi.)	100	12	17.56
12.	1 mg	No base	100	12	0
13.	1 mg	K ₂ CO ₃ (1 equi.)	30-100	12-6	100
14.	1 mg	K ₂ CO ₃ (1 equi.)	30	5	81.81
15.	1 mg	K ₂ CO ₃ (1 equi.)	30	3	47.36
16.	1 mg	K ₂ CO ₃ (1 equi.)	30	1	20.80

Table 6.A7: Optimization of Base, Temperature and time, **Reaction conditions:** Iodobenzene (1.59 mmol), Phenylboronic acid (1.59 mmol), Water (solvent) (10 ml), TLC (n-hexane), GC-MS (HPLC grade chloroform), Yields were obtained by GC-MS analysis

GC MS spectra during Optimization of base for the reaction between iodo benzene and phenylboronic acid (Figure 6.A3)



Figure 6.A3: GC-MS spectra of the product for Pd@IO-DTPA-DNA catalysed reaction between iodobenzene and phenylboronic acid performed using different bases and in Water as a solvent

GC MS spectra during Optimization of base amount for the reaction between iodobenzene and phenylboronic acid (Figure 6.A4)

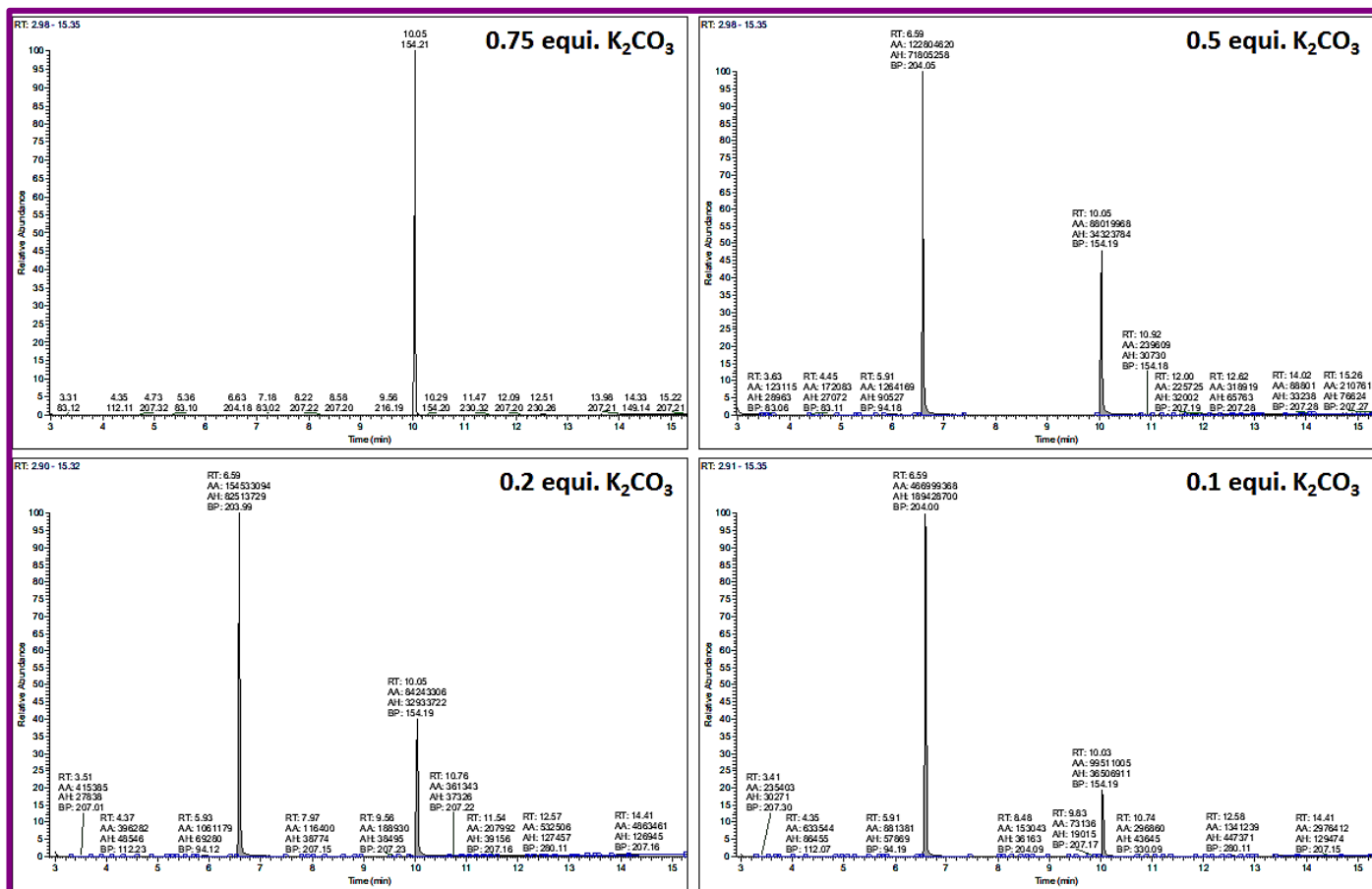


Figure 6.A4: GC-MS spectra of the product for Pd@IO-DTPA-DNA catalysed reaction between iodobenzene and phenylboronic acid performed using different amount of K_2CO_3 and Water as a solvent

GC MS spectra during Optimization of Time for the reaction between iodobenzene and phenylboronic acid (Figure 6.A5)

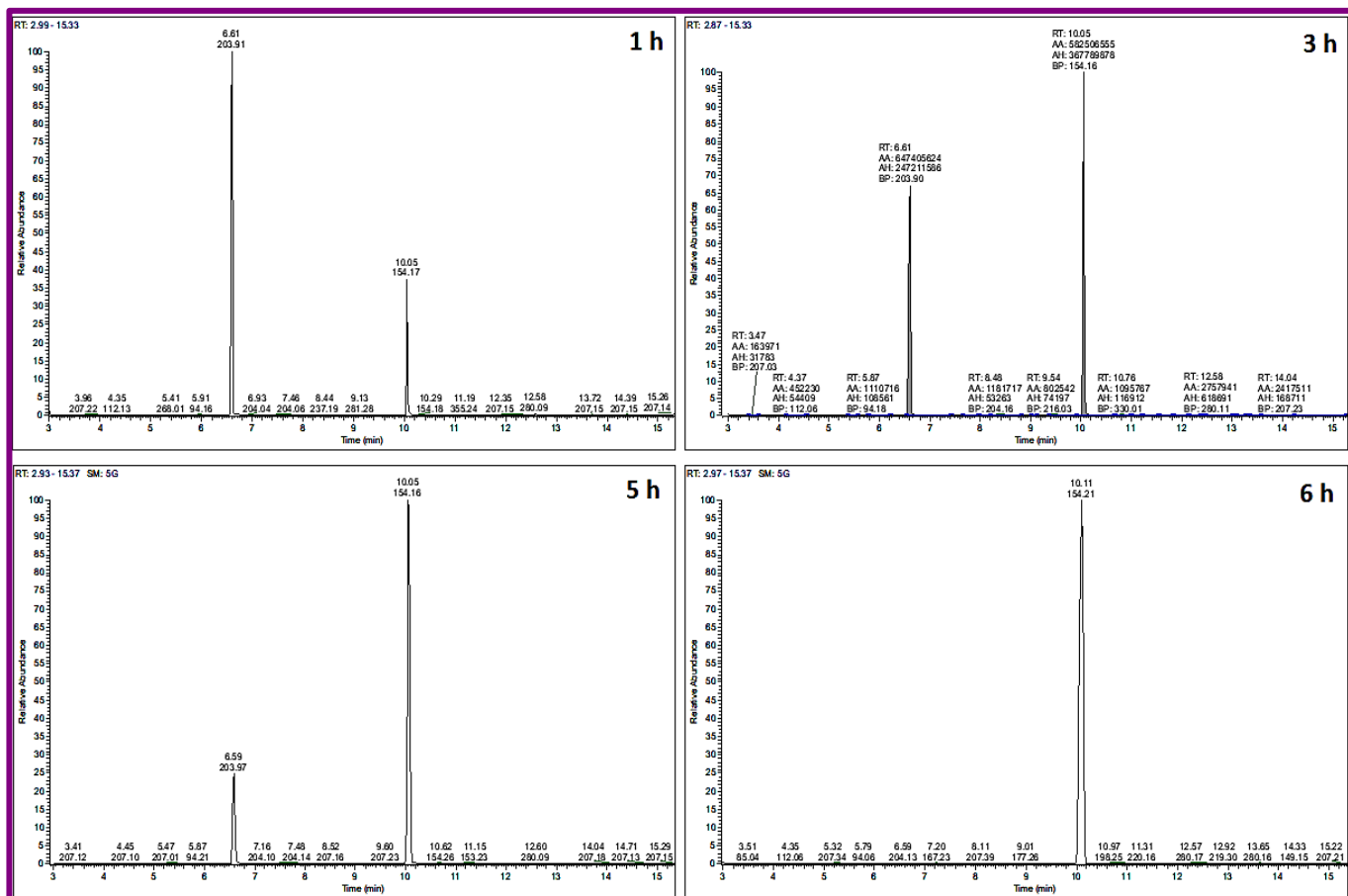
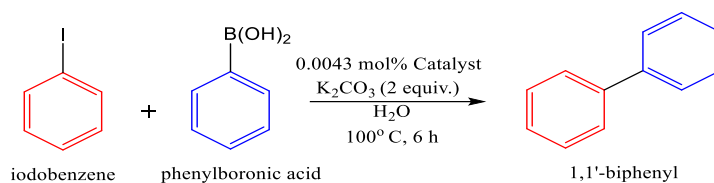


Figure 6.A5: GC-MS spectra of the product for Pd@IO-DTPA-DNA catalysed reaction between iodobenzene and phenyl boronic acid performed at 35 °C in the time range 1 to 6 hours



M.P: 70 °C

Molecular weight: 154.21 gm/mol

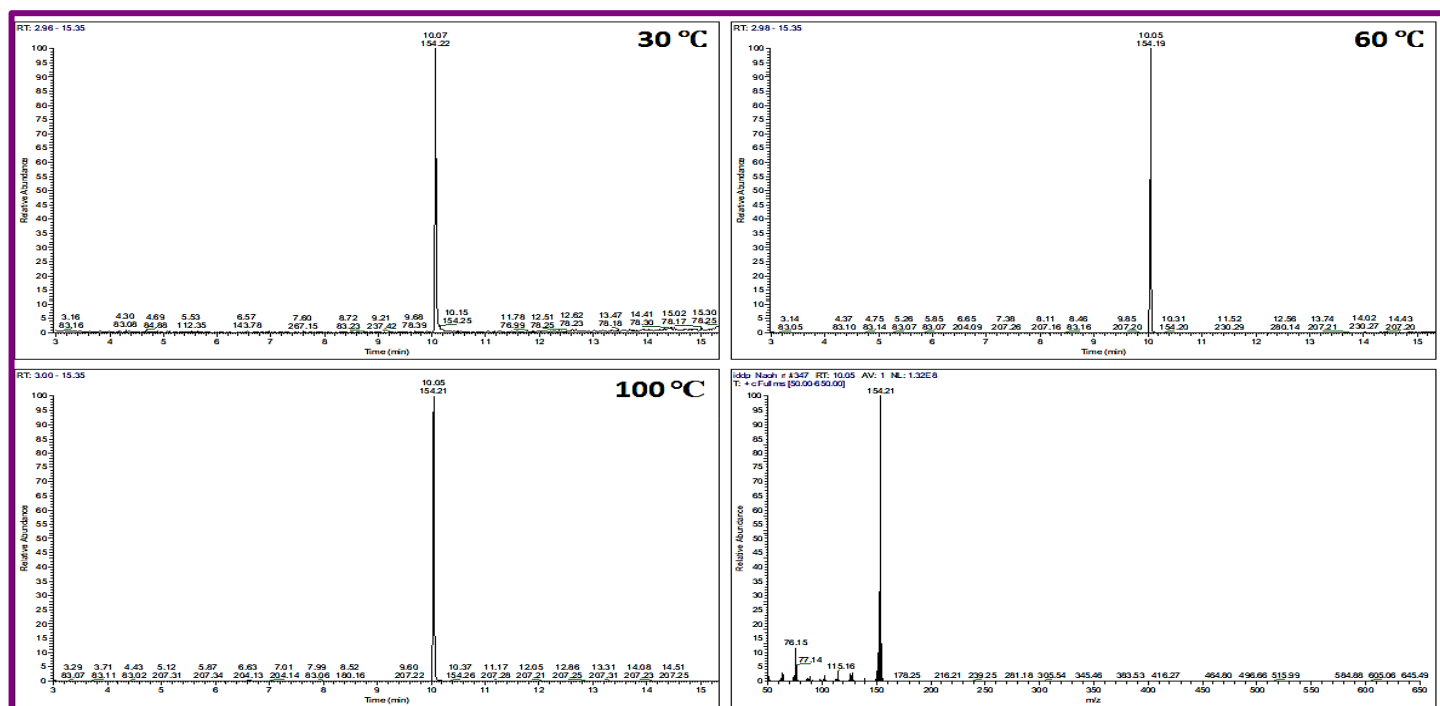


Figure 6.A6: GC-MS spectra of crude product (Biphenyl) synthesized From Iodobenzene at RT, 60°C and 100 °C

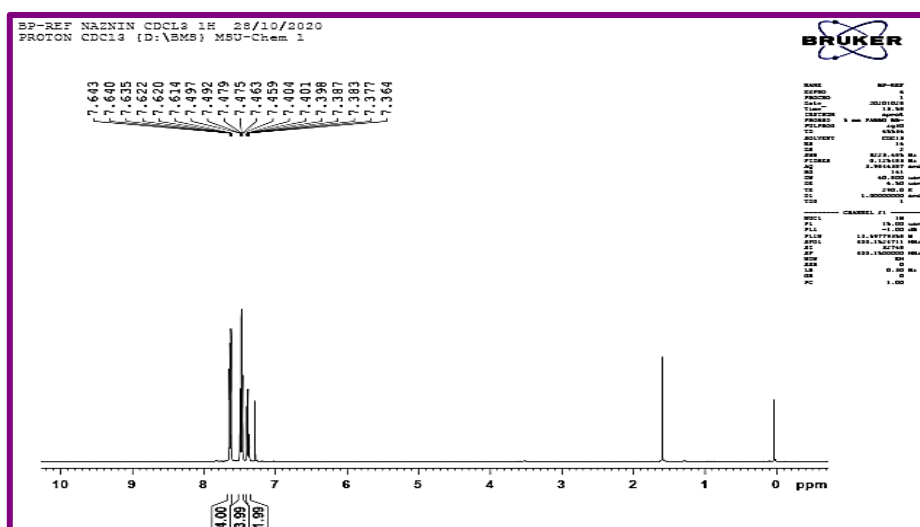
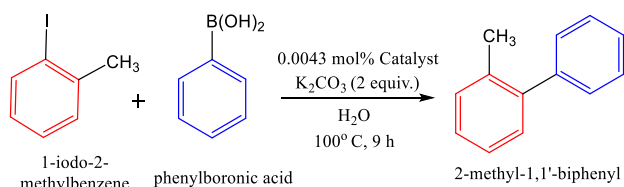


Figure 6.A7: NMR spectra of column purified (Biphenyl) synthesized From Iodobenzene



B.P: 255 °C

Molecular weight: 168.24 gm/mol

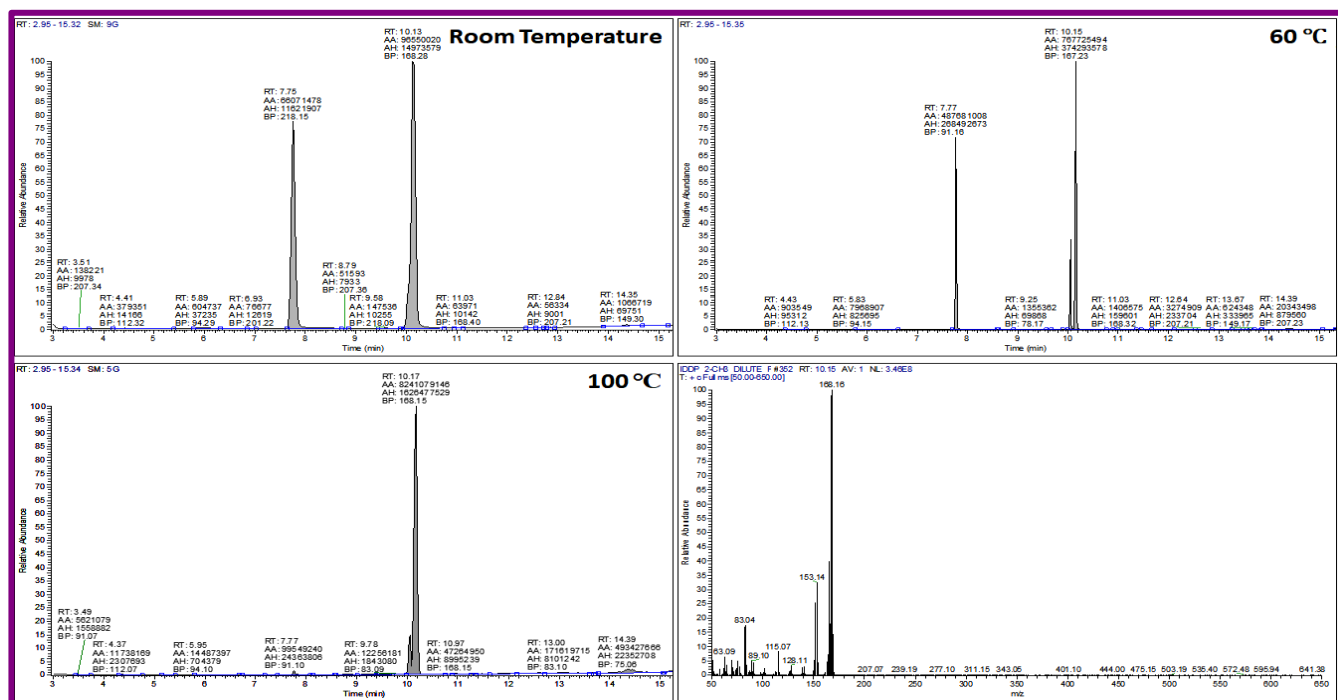


Figure 6.A10: GC-MS spectra of crude product (2-methyl-1,1'-Biphenyl) synthesized at RT, 60°C and 100 °C

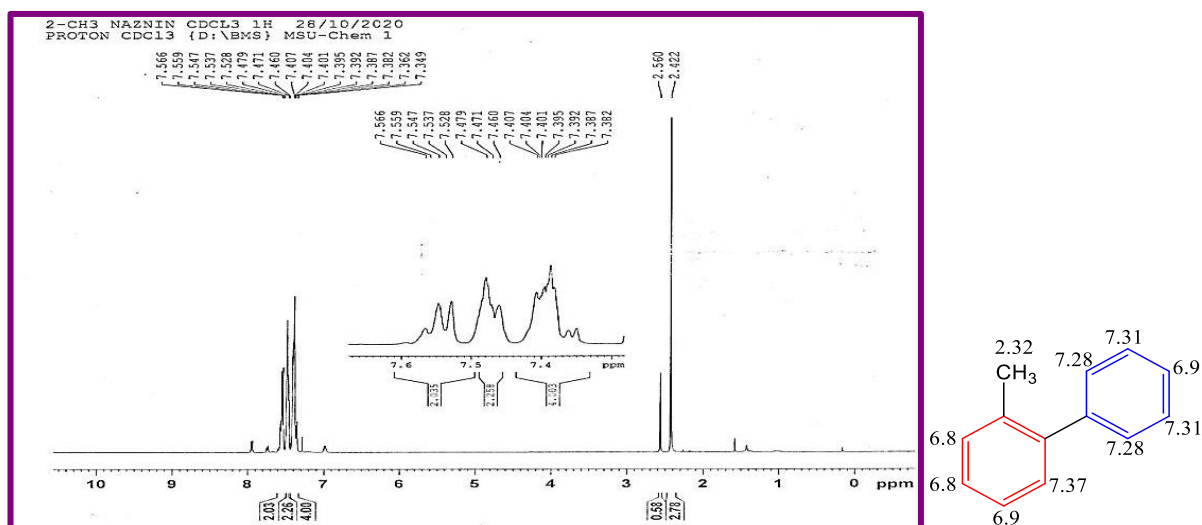
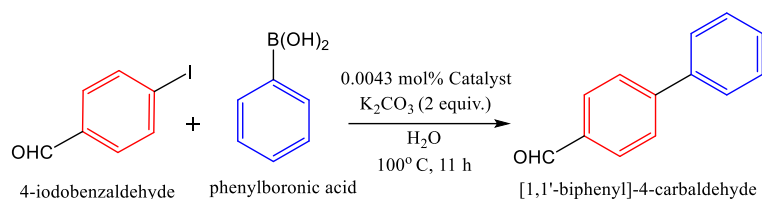


Figure 6.A11 NMR spectra of column purified (2-methyl-1,1'-Biphenyl)



M.P. 60 °C

Molecular weight: 182.2 gm/mol

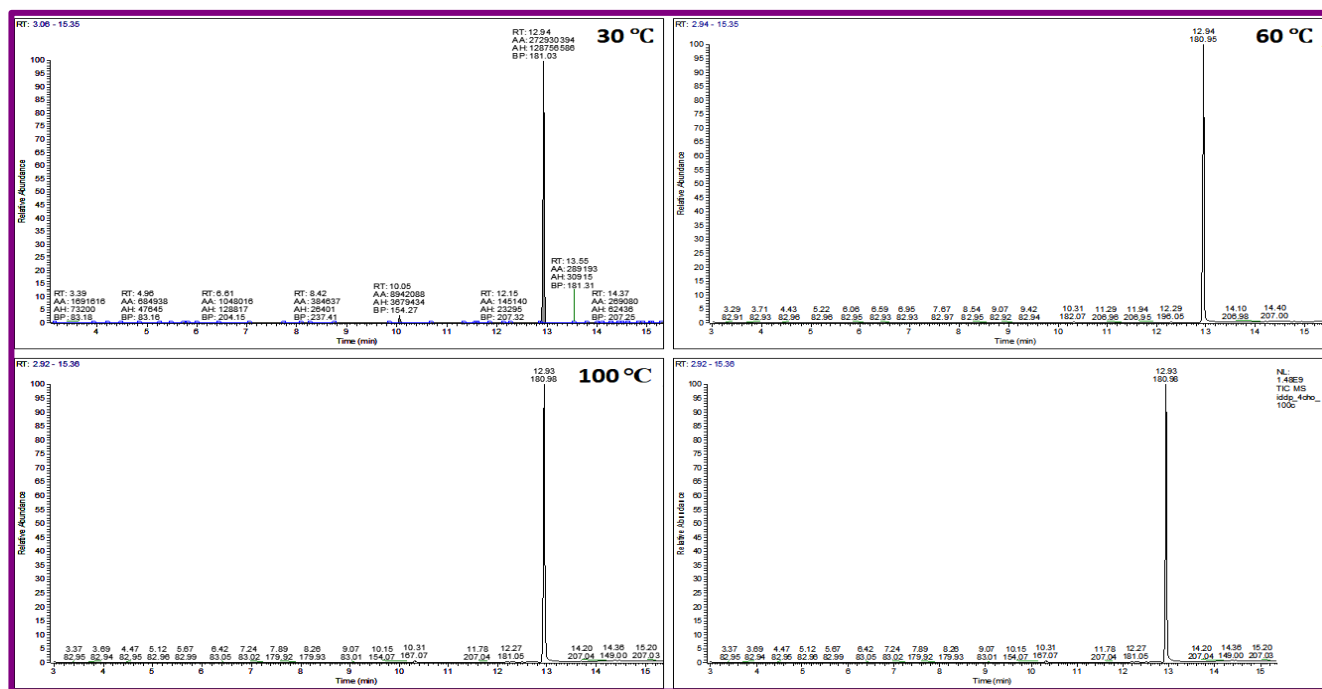


Figure 6.A12: GC-MS spectra of crude product ([1,1'-biphenyl]-4-carbaldehyde) synthesized at RT, 60°C and 100 °C

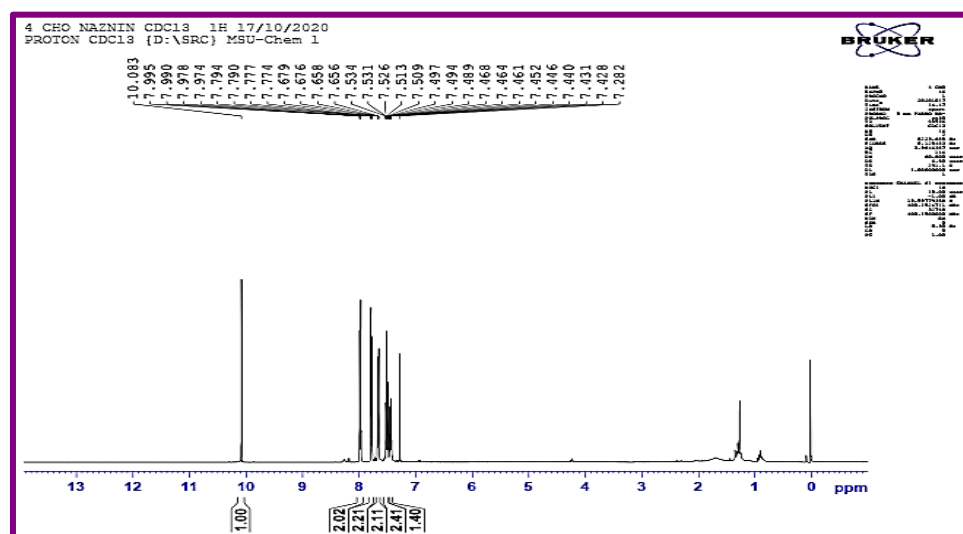
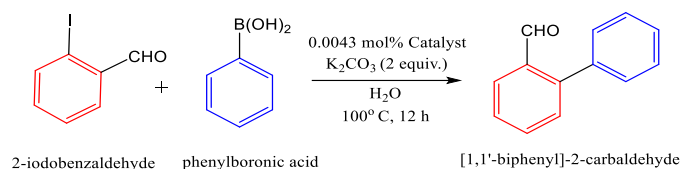


Figure 6.A13: NMR spectra of column purified ([1,1'-biphenyl]-4-carbaldehyde)



B.P: 90 °C

Molecular weight: 182.2 gm/mol

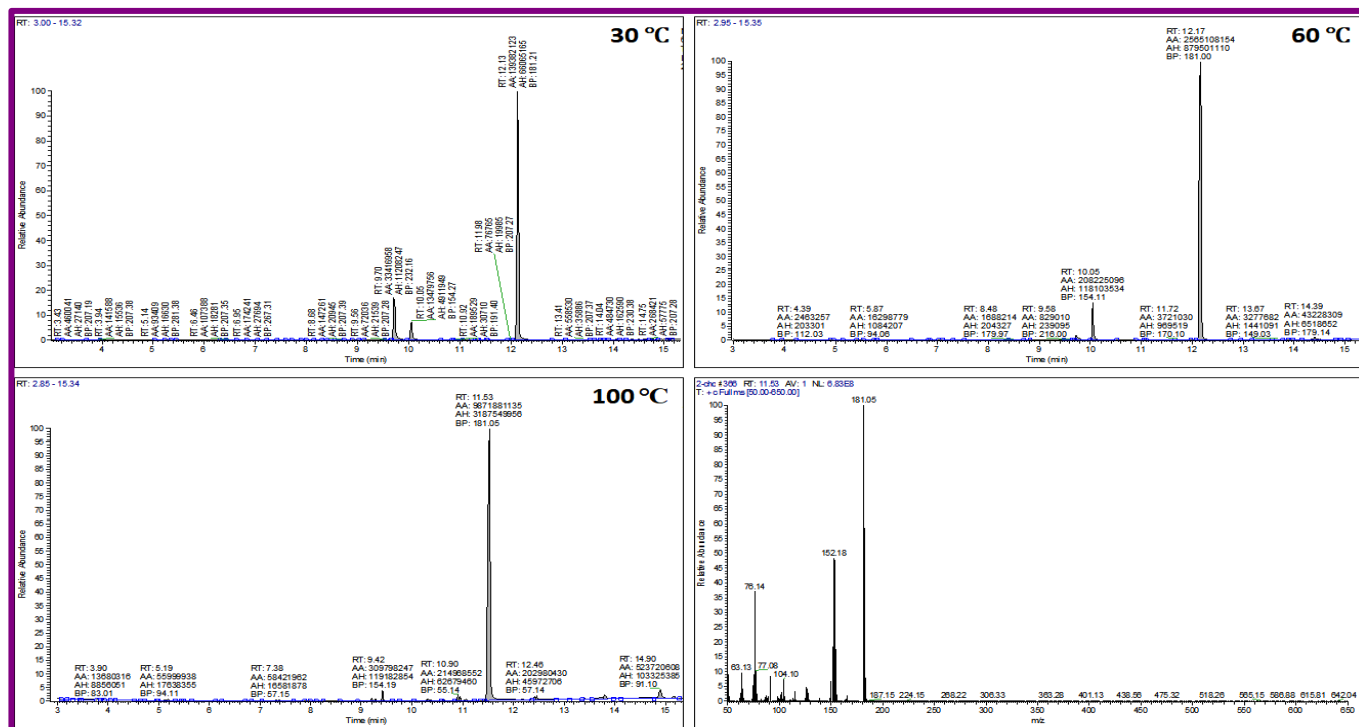


Figure 6.A14: GC-MS spectra of crude product ([1,1'-biphenyl]-2-carbaldehyde) synthesized at RT, 60°C and 100 °C

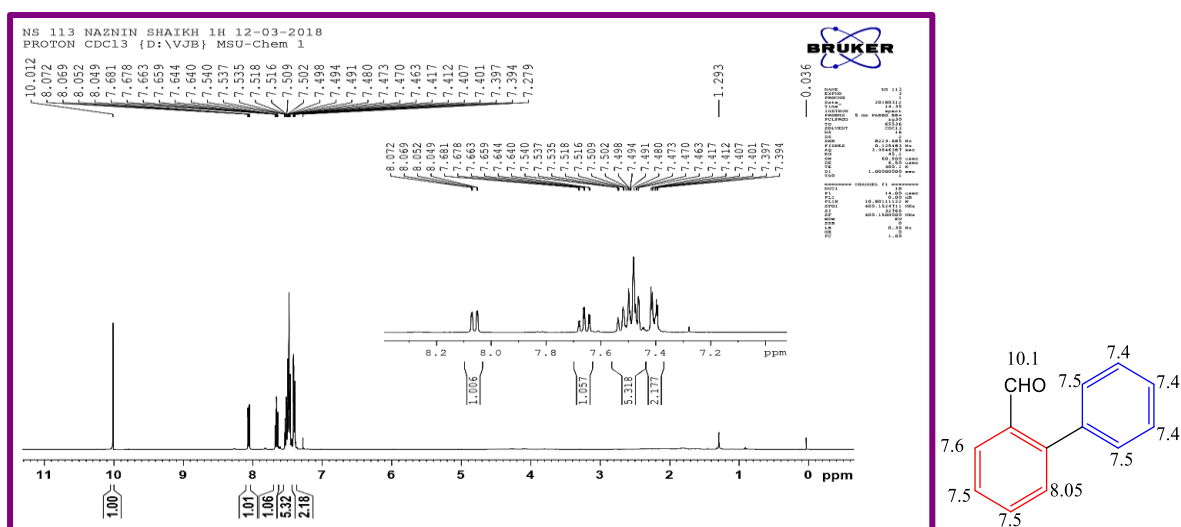
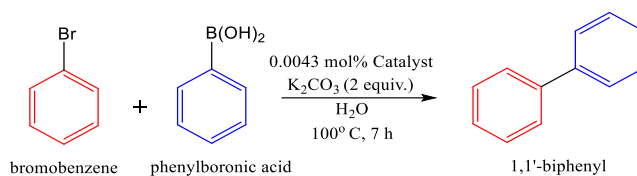


Figure 6.A15: NMR spectra of column purified ([1,1'-biphenyl]-2-carbaldehyde)

M.P: $70^\circ C$

Molecular weight: 154.21 gm/mol

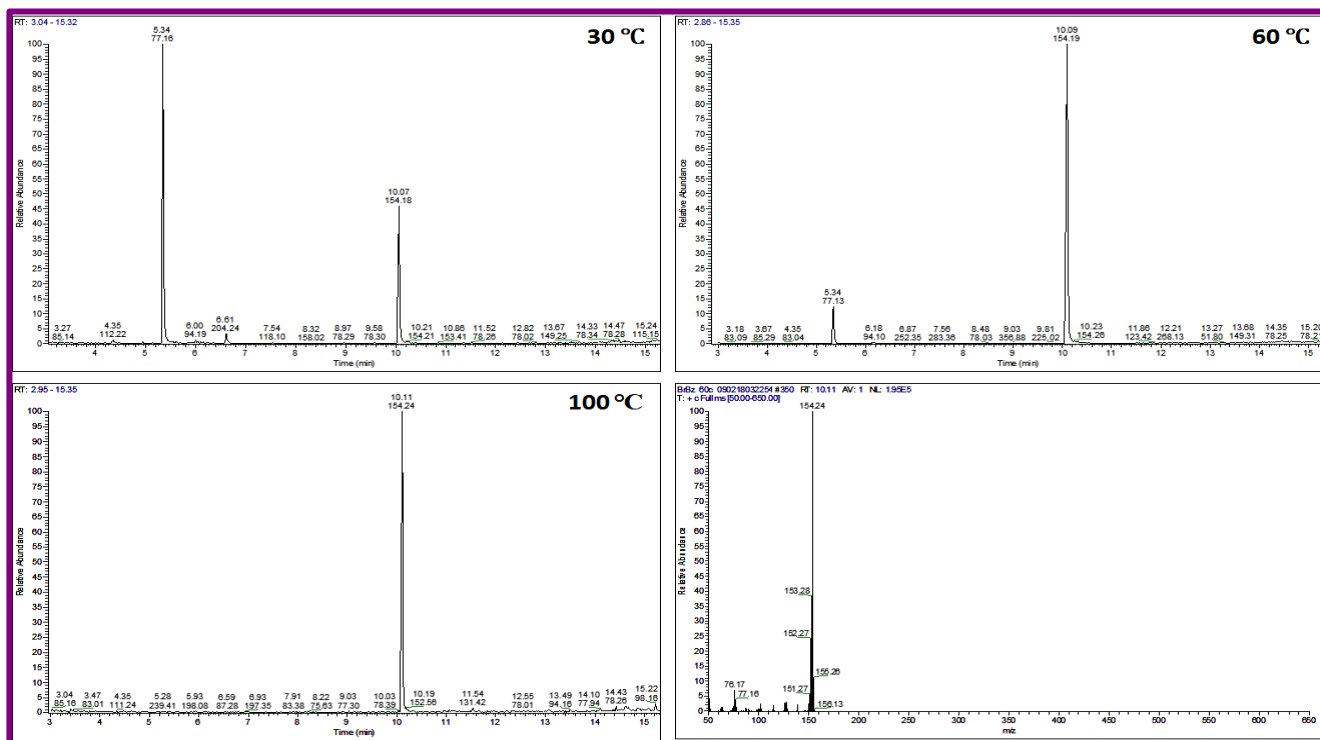


Figure 6.A16 GC-MS spectra of crude product (Biphenyl) synthesized From Bromobenzene at RT, $60^\circ C$ and $100^\circ C$

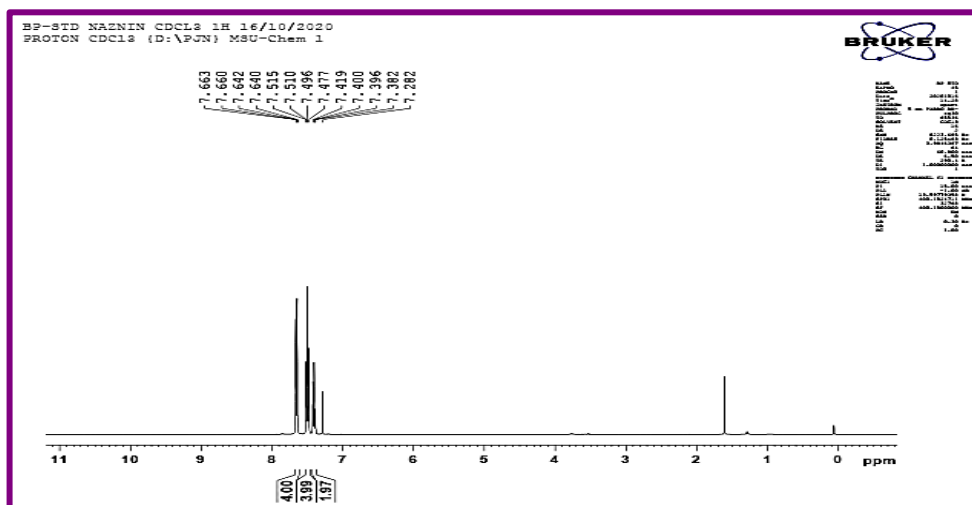
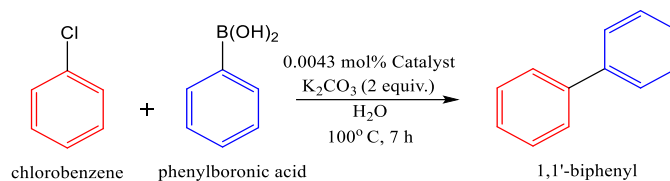


Figure 6.A17 NMR spectra of column purified Biphenyl synthesized From Bromobenzene



M.P: 70 °C

Molecular weight: 154.21 gm/mol

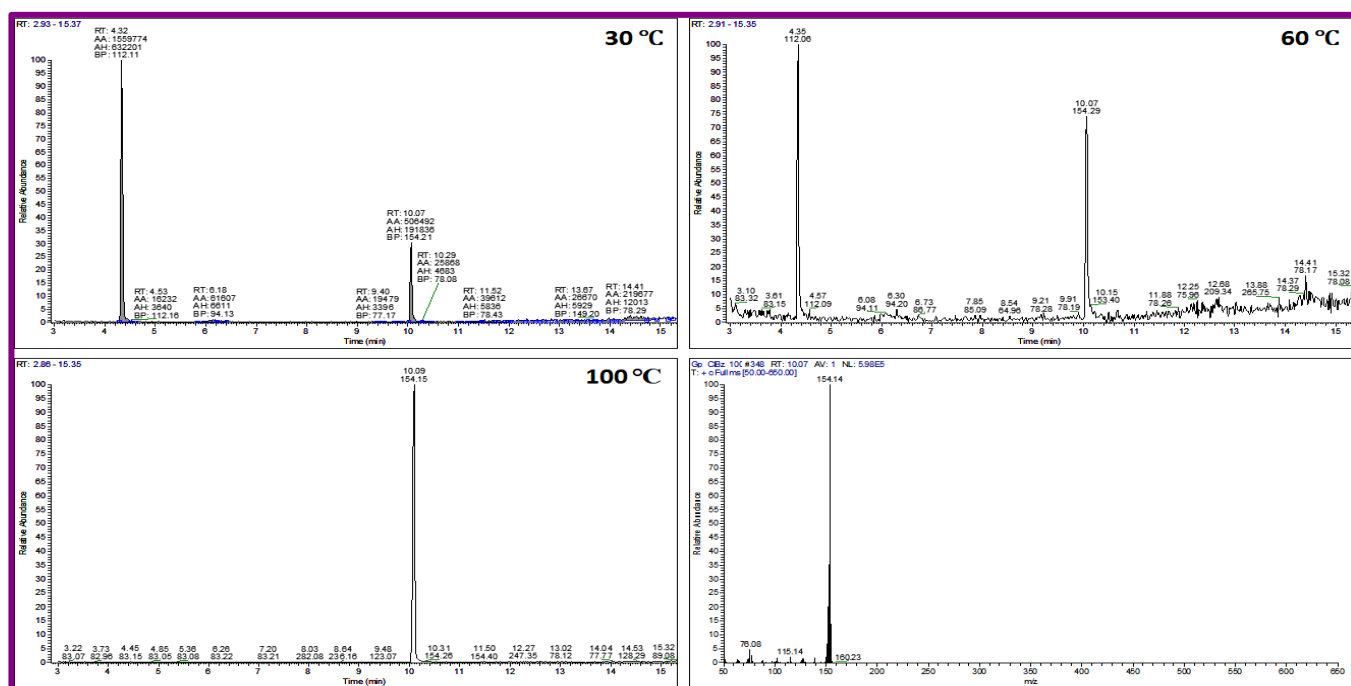


Figure 6.A18 GC-MS spectra of crude product (Biphenyl) synthesized From Chlorobenzene at RT, 60°C and 100 °C

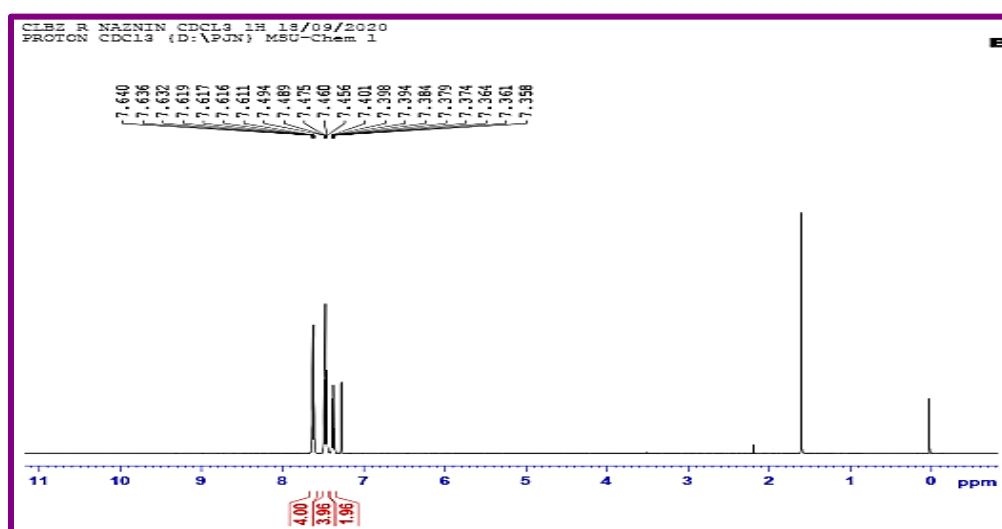
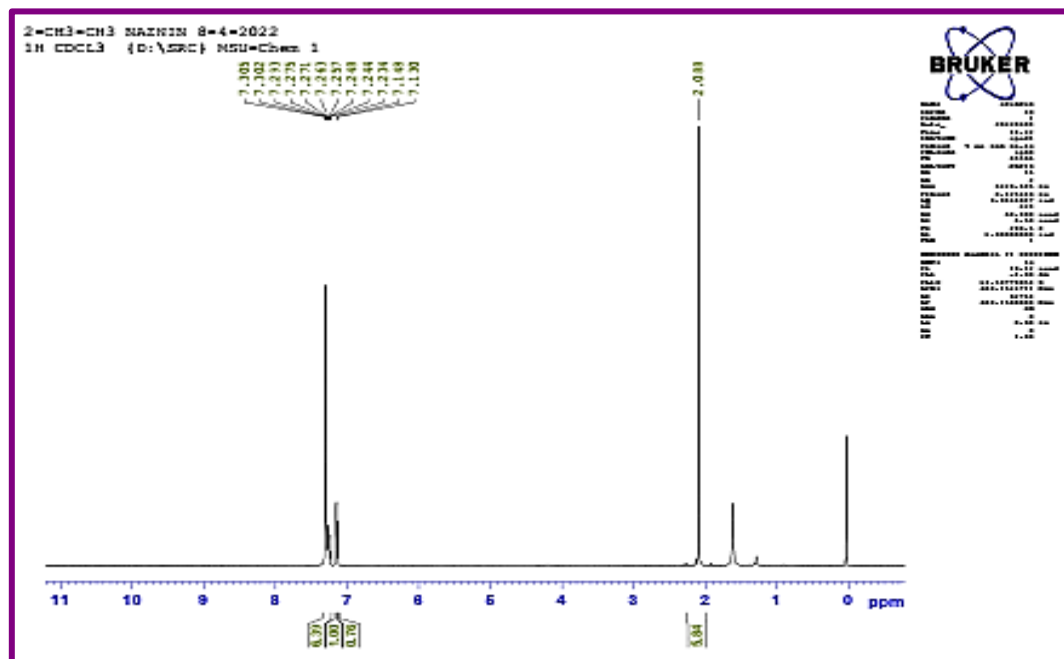
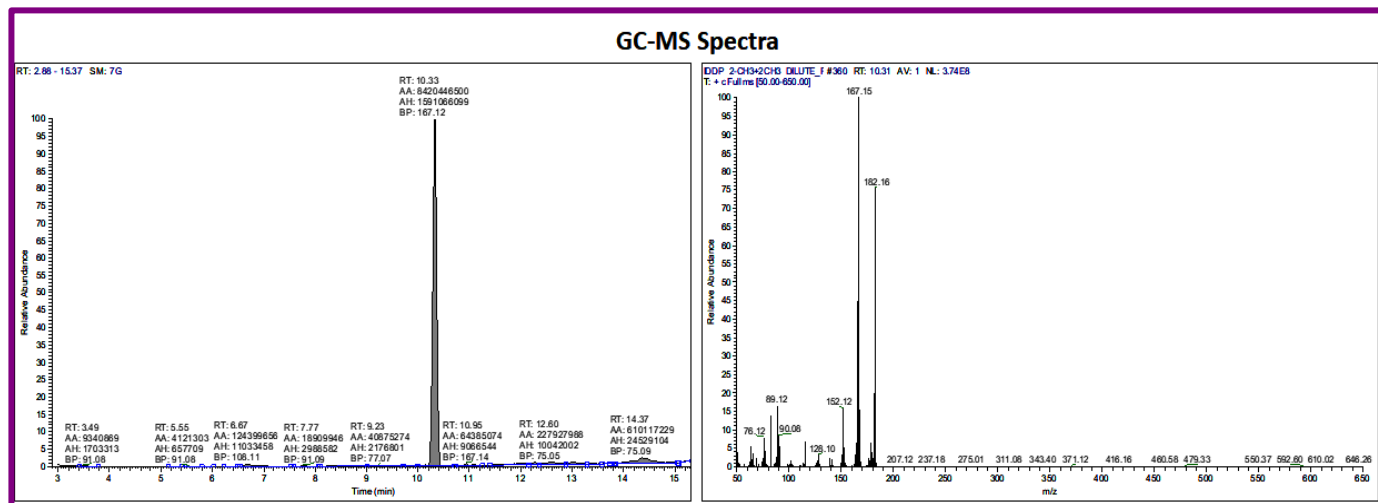
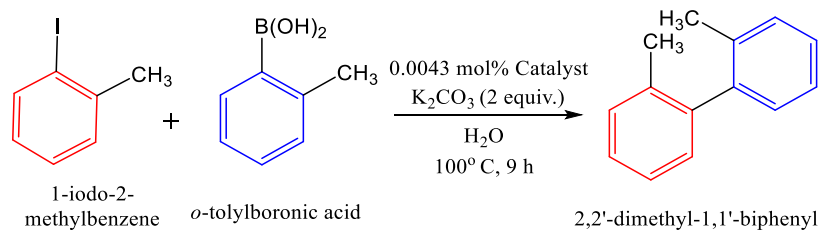


Figure 6.A19 NMR spectra of column purified Biphenyl synthesized From Chlorobenzene



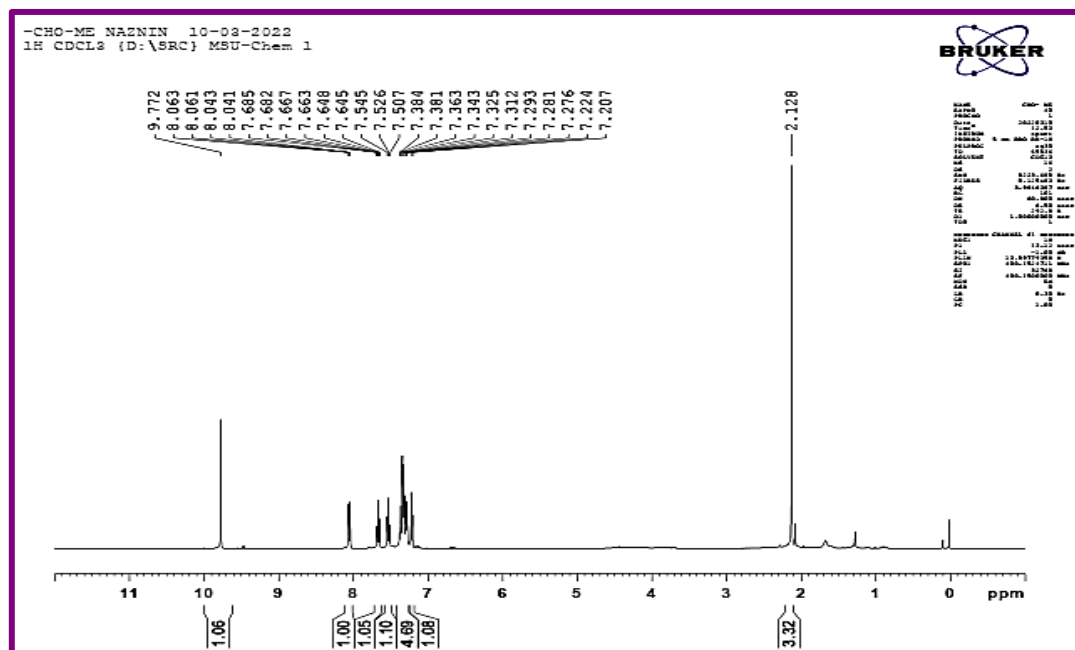
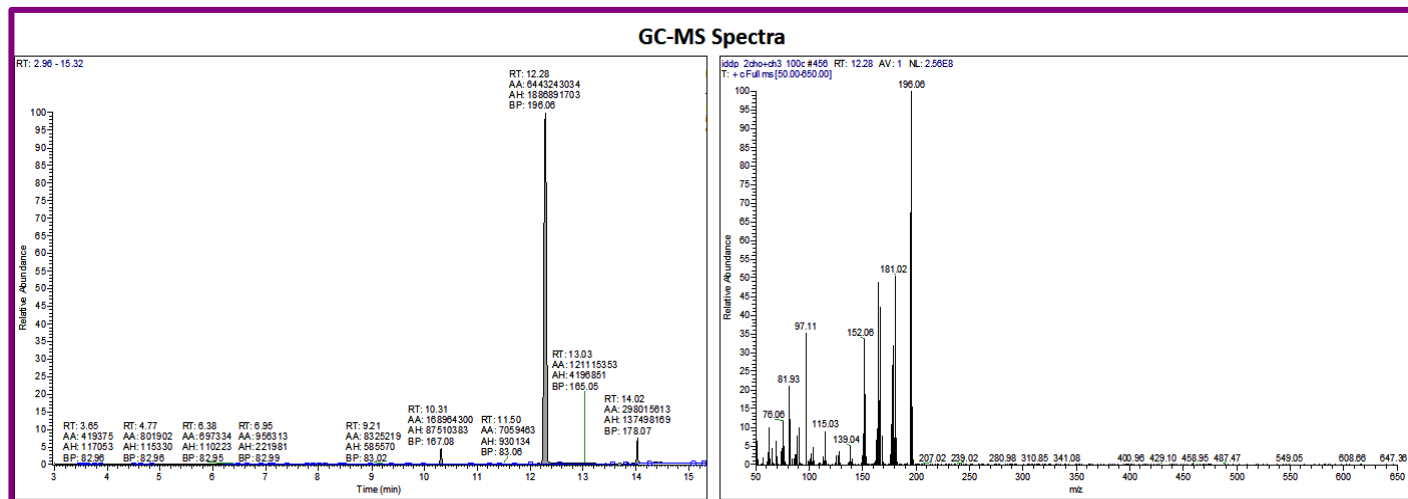
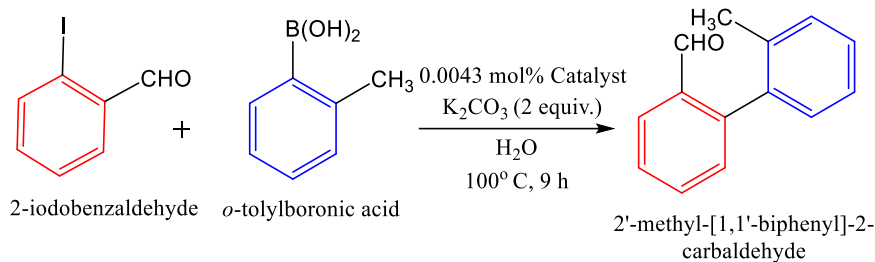


Figure S6.21 GC-MS and NMR spectra of 2'-methyl-[1,1'-biphenyl]-2-Carbaldehyde

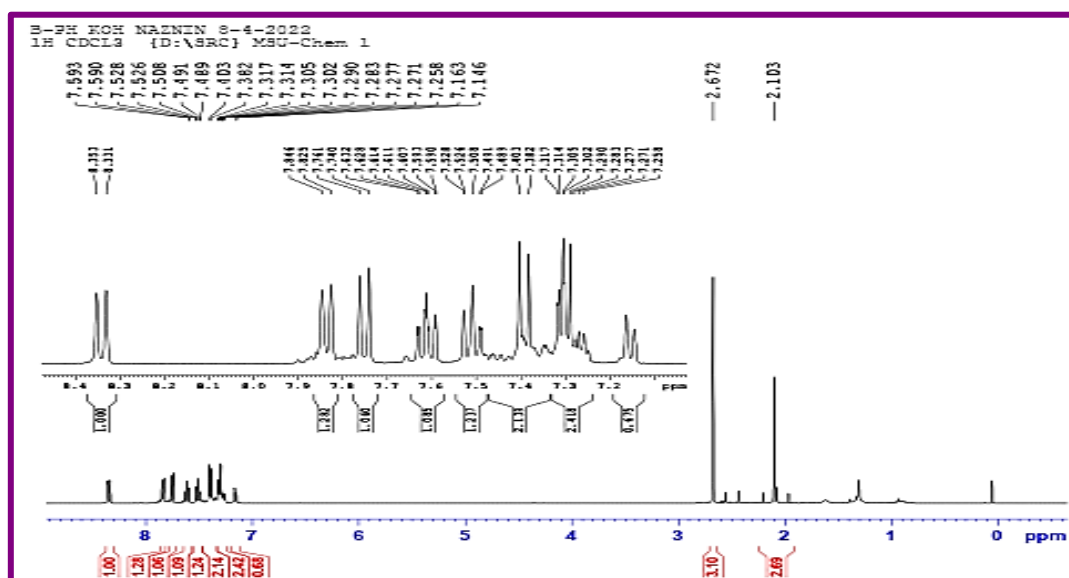
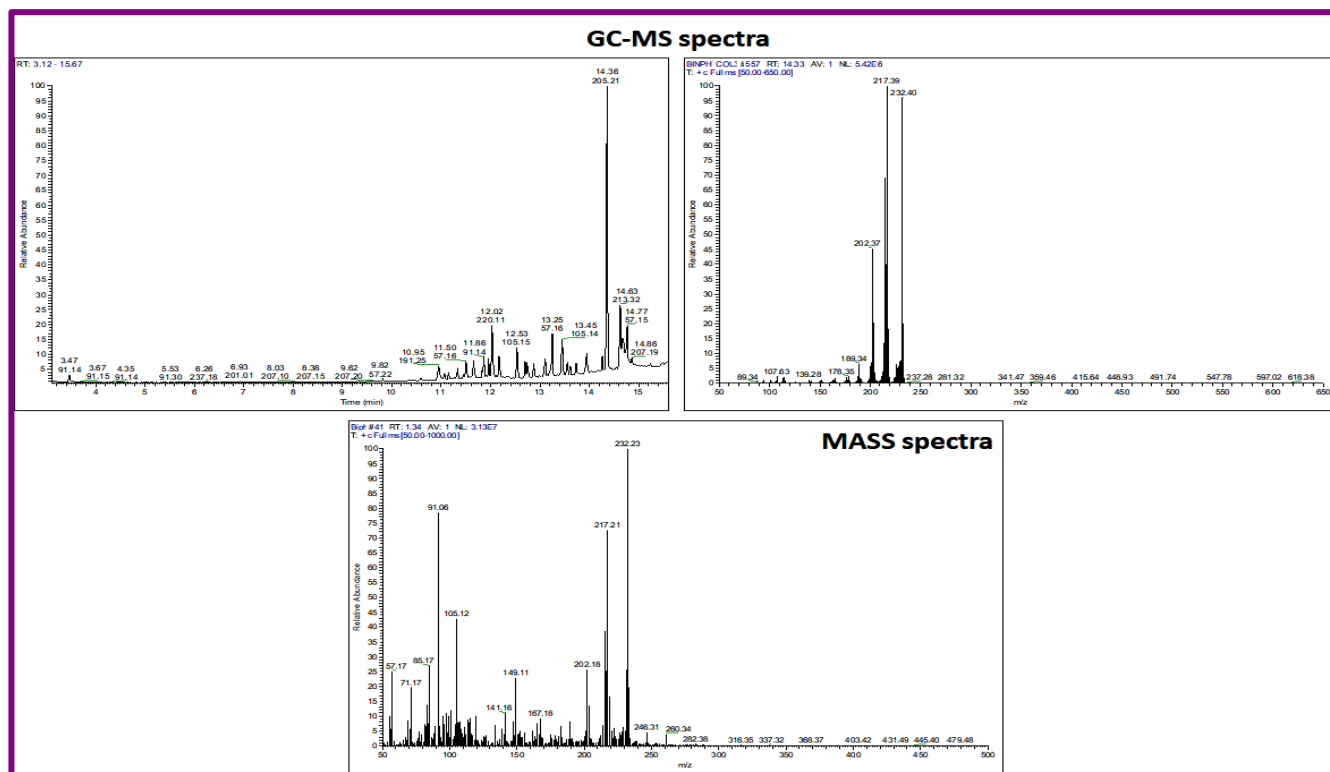
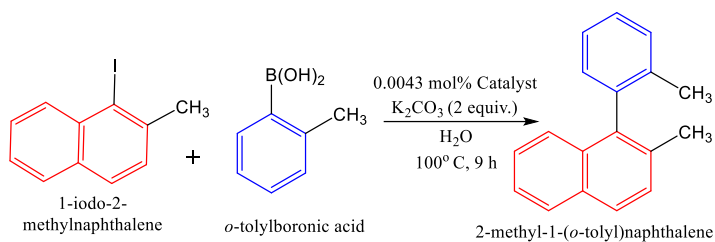


Figure S6.22 GC-MS, MASS and NMR spectra of 2-Methyl-1-(*o*-tolyl)naphthalene

Hot Filtration test

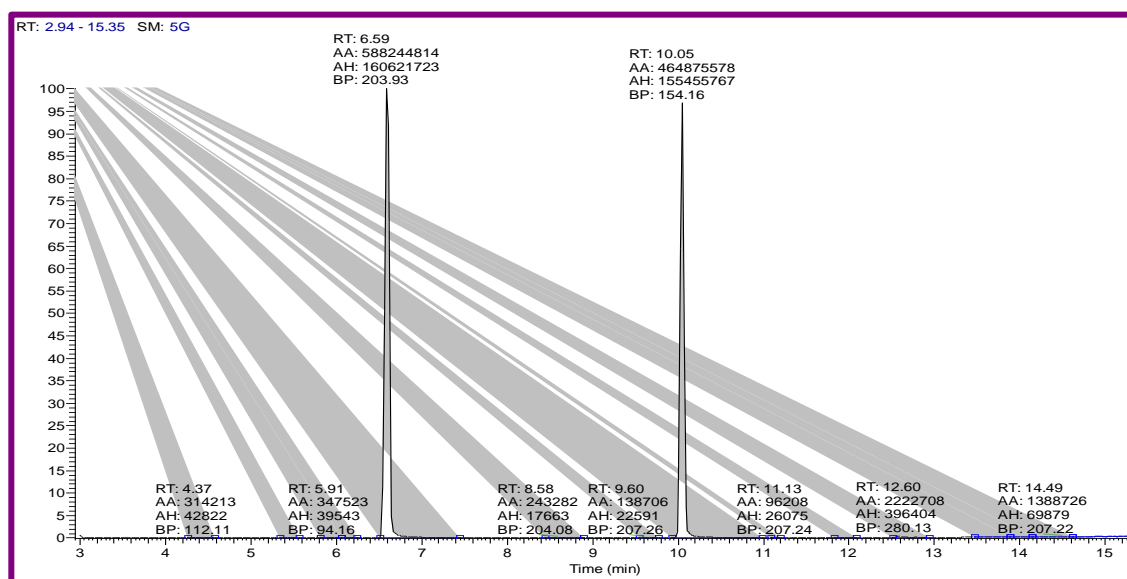


Figure 6.A23: GC-MS spectra of hot filtration study after 3 hrs.

Recyclability of the catalyst: Recycling of catalyst was carried out using Iodobenzene (1.59mmol), Phenyl boronic acid (1.59 mmol), K_2CO_3 (1.59 mmol), Pd@IO-DTPA-DNA (1 mg) and H_2O (10 ml) at 90-100 °C under stirring for 6 h. Pd@IO-Chitosan maintained its activity upto 19 cycles. A 1.9% decrease in yield was observed during the 19th cycle. (Figure S26)

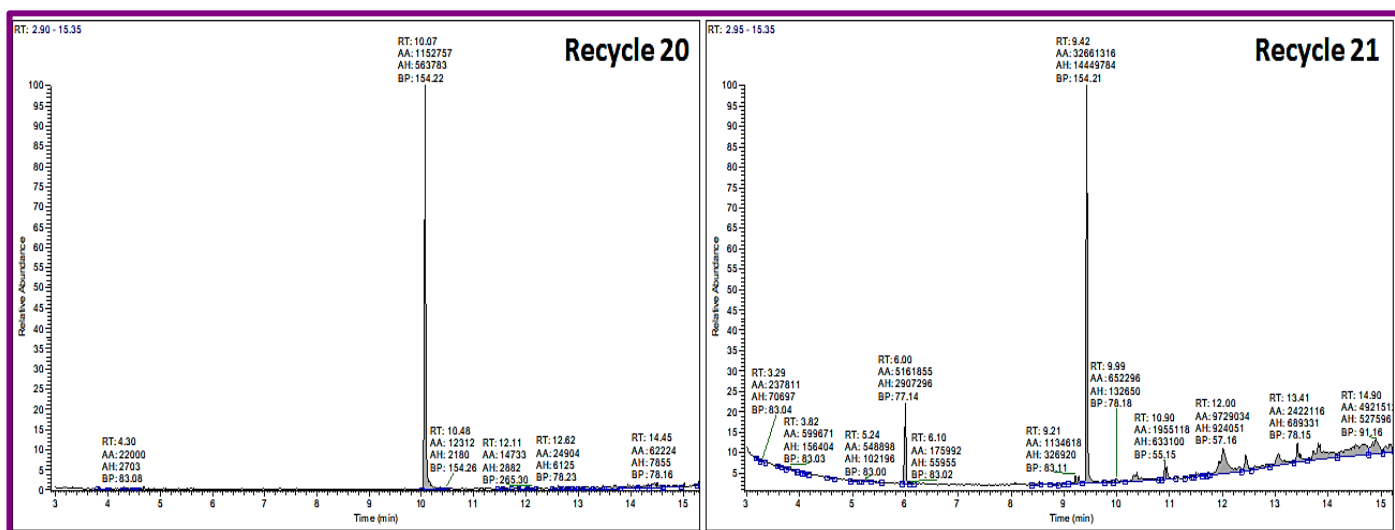


Figure 6.A24: GC-MS spectra of recycling study